Alma Mater Studiorum – Università di Bologna

DOTTORATO DI RICERCA IN

Scienze Biochimiche e Biotecnologiche

Ciclo XXIX

Settore Concorsuale di afferenza: 05/G1

Settore Scientifico disciplinare: SSD BIO/14

“Neuroprotective role of N-acylphosphatidylethanolamines in Parkinson’s disease”

Presentata da: Francesca Palese

Coordinatore Dottorato	**Relatore**
Prof. Santi Mario Spampinato	**Prof. Daniele Piomelli**

Esame finale anno 2017

ABSTRACT

N-acylphosphatidylethanolamines are a class of phospholipids present at low concentrations in cellular membranes[1]. They have been studied as fatty-acid ethanolamine (FAEs) precursors, given FAEs bioactive effects such as control of inflammation[2], pain sensation and neuroprotection[3] as well as control of food intake[4].

However, NAPEs may also have biological functions of their own: they might participate in the control of membrane fluidics[5], organization of lipid raft[5], arrangement of cell division site domains[7] and protein anchorage.

Evidence indicates that NAPEs are produced in the brain following injurious stimuli of diverse nature. Ischemia[8], excitotoxicity[9] as well as toxic molecules including sodium azide[10], glutamate[11] and ethanol[12] may all cause NAPE accumulation.

In this context, we have recently observed that this lipid molecules are increased following the administration of the neurotoxin 6-hydroxydopamine in mice[13], a widely used model of Parkinson's disease.

Parkinson's disease is a chronic progressive neurodegenerative disease caused by the loss of the nigrostriatal dopaminergic neurons[14], which results in an impairment of the control of voluntary movements, leading to a motor symptomatology that includes bradykinesia, rest tremor, rigidity and postural disturbances[15].

Parkinson's disease as well as other neurodegenerative diseases represent a substantial burden for public health, given the fact that worldwide population is getting older and these pathologies mostly affect elderly people. Unfortunately to date no therapies have been developed to cure neurodegenerative disease. Thus, there is the need to understand in greater depth Parkinson's disease pathophysiology and to further develop new therapeutic approaches for this condition.

The aim of the present work was to elucidate whether and how NAPE production is involved in the neurodegenerative process.

Using a combination of genetic, pharmacological and behavioral techniques, I was able to show that locally produced NAPEs exert protective effects against 6-OHDA-induced toxicity by regulating the expression and activity of LRRK2, a multifunctional protein that is known to be involved in both familial and sporadic Parkinson's.

The evidence collected in my experiments may thus provide a starting point for the development of new therapeutic approaches for neurodegenerative disease, as well as for the identification of biological markers useful in the early detection of these pathological diseases.

INTRODUCTION

1. N-ACYLPHOSPHATIDYLETHANOLAMINE

N-acylphosphatidylethanolamines are triacylated phospholipids derived from phosphatidylethanolamine (PE) with a third, N-linked fatty acyl chain[16], generally referred to by the acronym NAPE. Although in small amounts, NAPEs are a class of widely expressed glycerophospholipids, present in both eukaryotic, plant and animal cells, as well as in prokaryotic cells.

Under physiological conditions, NAPEs represent only 0.01% of total phospholipids, with levels in the range of nmol/g of wet tissue, and a little higher expression in the brain. Besides the brain, they are found in other organs such as spinal cord, testis and spleen as well as physiological fluids[17]. NAPEs are located in cellular membranes and are more abundant in the plasma membrane than in intracellular ones[1]. Furthermore, they have been detected in human plasma where they are probably associated with the outer phospholipid shell of lipoproteins[18].

1.1 NAPE biosynthesis

The canonical pathways for the biosynthesis and hydrolysis of NAPE species were thought to be relatively simple, however recent studies have shown that the pathways are more complicated than expected, as every reaction is often catalyzed by diverse enzymes or isoenzymes.

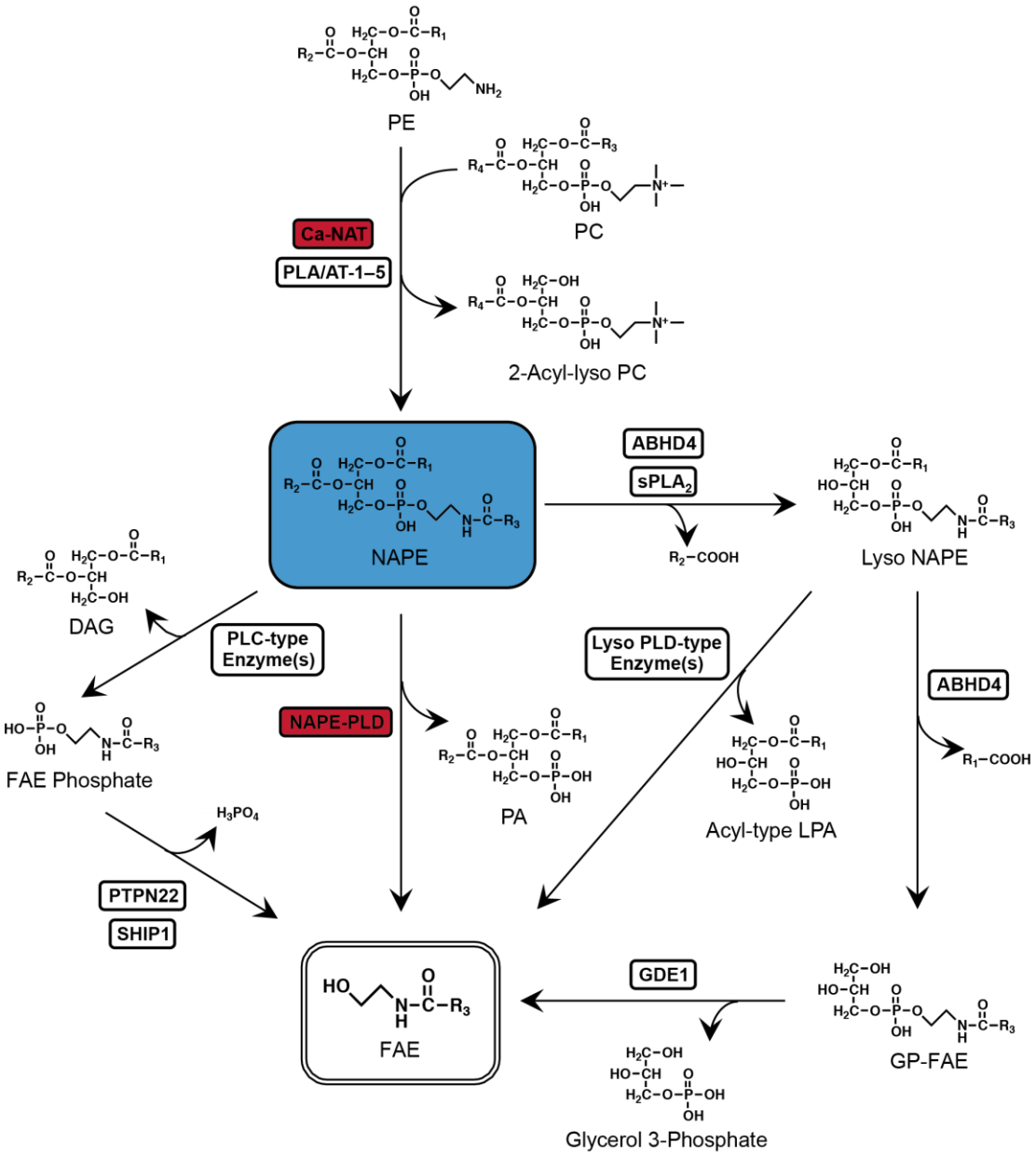

Figure 1: Biosynthetic and catabolic pathway of NAPE.

NAPE biosynthesis, as summarized in Fig. 1, consists in the transfer of a fatty acyl chain from *sn*-1 position of a donor glycerophospholipid molecule such as phosphatidylcholine (PC) to the primary amino group of phosphatidylethanolamine (PE) by the action of the Ca^{2+}-dependent enzyme N-Acyltransferase (Ca-NAT)[19]. This enzyme is an integral membrane protein[16] found in mammalian tissue including brain[20], heart and testis. Among various brain regions in rat, the highest activity of Ca-NAT was observed in brainstem, followed by intermediate activity in the striatum among other areas[20]. Ca-NAT does not discriminate based on the length or unsaturation of the transferred acid chain. This is why saturated fatty acyl chains

(abundant in the *sn-1* position of glycerophospholipids) are preferred over polyunsaturated fatty acyl chains (abundant in the *sn-2* position) as the molecular species of N-acyl groups of NAPE[21].

Another Ca^{2+}-independent pathway for NAPEs synthesis has been discovered[22]: five members of the HRAS-like suppressor (HRASLS) superfamily possess phospholipid-metabolizing activities including NAPE-forming N-acyltransferase activity, which releases an acyl group from the *sn-1* or *sn-2* position of PC to PE in a Ca^{2+}-independent manner. These enzymes also have O-acyltransferase activity, which transfers an acyl group from PC to the hydroxyl group of lyso-PC as well as PLA_1/A_2 activity, which hydrolyzes the *sn-1* or *sn-2* ester bonds of PC or PE.

They have been denominated phospholipase A/acyltransferase (PLA/AT)-1-5. The PLA/AT-1, PLA/AT-2 and PLA/AT-5 isoforms showed higher N-acyltransferase activities over PLA_1/A_2 activities compared to PLA/AT-3 and PLA/AT-4. All five HRASLS enzymes are expressed in testis, liver, adipose tissue and kidney, but in contrast to Ca-NAT, their brain levels are low[23].

1.2 NAPE hydrolysis

The hydrolysis of NAPEs occurs via multiple enzyme-mediated routes (Fig. 1). The primary pathway consists in the release of their third acyl chain (*N*), and the simultaneous formation of fatty acid ethanolamides (FAE) and phosphatidic acid, through the action of N-acyl phosphatidylethanolamine-specific phospholipase D (NAPE-PLD)[24]. Depending on the length and the saturation of the acyl chain, diverse FAEs can be produced, as illustrated in Fig. 2. The fatty acid composition of the N-acyl group is dominated by saturated fatty acids (palmitic and stearic acid, 16:0 and 18:0, respectively) and to a lesser extent oleic acid 18:1, while arachidonic acid 20:4 usually accounts for 0.4-0.6% of the fatty acids[21]. FAEs include anandamide (AEA), palmitoylethanolamide (PEA), oleoylethanolamide (OEA) and stearoylethanolamide (SEA). All of them are important signaling molecules, having a variety of biological effects, including control of food intake, inflammation, pain sensation, and neuroprotection.

PEA is made of a saturated 16 carbon chain, and shows anti-inflammatory, analgesic and neuroprotective actions through its binding to peroxisome proliferator-activated receptor-α (PPAR-α)[2]; PPAR-α is also a target for OEA, a lipid composed by a monounsaturated chain of 18 carbons, that regulates satiety, body weight and cancer cell proliferation[4]; SEA is made by a saturated 18 carbons chain, and was shown to be pro-apoptotic and anorexic[16]; AEA, the least abundant FAE, contains a

polyunsaturated acyl chain of 20 carbons and 4 double bonds (20:4) and acts as a CB1 agonist to induce analgesia, neuroprotection, hypotension and appetite stimulation[16].

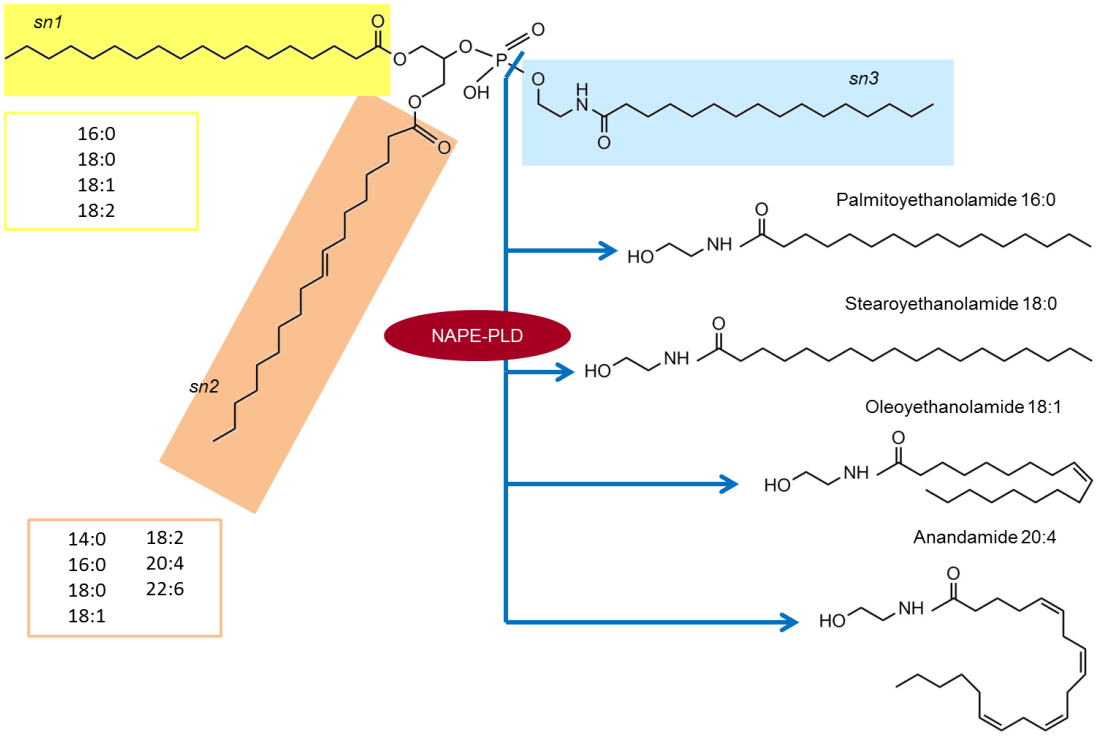

***Figure 2: FAE generation from NAPEs**. The sn1, 2 and 3 chains indicated in the picture are representative. The sn1 chain can be composed of 16:0, 18:0, 18:1 and 18:2, with 18:0 as the most abundant. Sn2 may be shows 14:0, 16:0, 18:0, 18:1, 18:2, 20:4 and 22:6, where 20:4 is the most expressed in nature. Sn3 when released by NAPE-PLD action give rise to FAEs, among others the most expressed and biological active are palmitoylethanolamine (16:0), stearoylethanolamine (18:0), oleoylethanolamine (18:1) and anandamide (20:4).*

NAPE-PLD is a member of the zinc metallohydrolase family of the β-lactamase[24], with a structure unrelated to any other PLD isoforms. NAPE-PLD is ubiquitously expressed at high levels in testis, kidney and brain[24]. The crystal structure of NAPE-PLD was obtained in our laboratory and reveals that the enzyme is tightly bound to microsomal and mitochondrial membranes through an extended lipid-binding surface spanning the NAPE-PLD dimer. Moreover, this enzyme shows a hydrophobic nook facing the lipid bilayer that provides a recognition filter: NAPE-PLD is highly specific for NAPEs without any selectivity for their N-acyl moieties[25]. Thus, its major physiological role appears to be non-specific formation of various FAEs including bioactive species.

The physiological regulators of NAPE-PLD activity are still unknown, and there is no evidence that the increase in intracellular Ca^{2+} concentration stimulates this activity. However, it has been shown that the proinflammatory bacterial endotoxin

lipopolysaccharide (LPS) suppresses the expression of NAPE-PLD and consequently down-regulates PEA biosynthesis in a human macrophage cell line[26].

The conversion from NAPE to FAE can occur also through multi-step pathways with the formation of an intermediate metabolite N-acylated lysophospholipids (lyso-NAPE)[27]. In these NAPE-PLD-independent pathways, an O-acyl chain of NAPE is eliminated to form lyso-NAPE, which is then subjected to the hydrolysis of the phosphodiester bond to generate FAE and lysophosphatidic acid (LPA). Alternatively, lyso-NAPE is further O-deacylated to form glycerophospho-FAE (GP-FAE), followed by hydrolysis of the phosphodiester bond to generate FAE and glycerol-3-phosphate[27].

1.3 NAPE-PLD KO mice

Ten years ago, Cravatt's group generated NAPE-PLD knockout mice (NAPE-PLD$^{-/-}$)[28]. These mice were born according to the expected Mendelian frequency and were viable and healthy without overt abnormality in cage behavior[28]. Moreover NAPE-PLD$^{-/-}$ mice showed 5-15 fold higher levels of NAPEs with saturated and monounsaturated N-acyl groups in the brain. However, the detection of unaltered or moderately reduced FAEs levels confirmed the existence of the alternative pathways for the biosynthesis of FAEs as described above[21]. In accordance with the presence of these NAPE-PLD-independent pathways, the brain of NAPE-PLD$^{-/-}$ mice showed a remarkable increase in endogenous levels of lyso-NAPE and GP-FAE as well as NAPE[21]. Moreover, deacylation of NAPE to lyso-NAPE could be catalyzed by secretory PLA_2s or by α/β-hydrolase domain-containing protein 4 (ABHD4). In addition, ABHD4 can further deacylate lyso-NAPE to produce GP-FAE. Glycerophosphodiester phosphodiesterase 1 (GDE1) mediates the hydrolysis of GP-FAE, resulting in the formation of FAE and glycerol-3-phosphate[29].

Double knockout mice of GDE1 and NAPE-PLD were generated in Cravatt's laboratory, and their brain levels of FAEs were compared with those of NAPE-PLD deficient mice[30]: interestingly, no differences were found between these mice. These results suggested the involvement of other enzymes in the NAPE-PLD-independent route. Indeed, there is a multi-step pathway to generate FAE through phospholipase C (PLC)-phosphatase activity. NAPE is hydrolyzed to produce FAE-phosphate, followed by dephosphorylation to generate FAE. Consistent with this signal route, mouse macrophage cells treated with LPS showed elevated levels of anandamide even though NAPE-PLD was downregulated[31]. PTPN22 and SHIP1 (Src homology

2 domain-containing inositol-5-phosphatase 1) were shown to exhibit phosphatase activity that produce anandamide from anandamide phosphate[16].

1.4 NAPE functions

NAPEs not only serve as precursors to FAEs, but also have biological functions on their own, as depicted in Fig. 3. First, NAPEs seems to work in membrane stabilization[5]. Indeed, the N-acyl chain of NAPE may be embedded in the membrane bilayer giving to this lipid a more membrane stabilizing structure than PE from which it derived. Having a negative charge, NAPE may lead to physiological functions in anchoring or activating various intracellular proteins[17]. Moreover, NAPEs do not seem to form cholesterol-rich domains, but they can displace cholesterol from cholesterol-sphingomyelin domains. Thus, when NAPEs are hydrolyzed to form FAEs, they may change cholesterol distribution in membranes, as FAEs can form 1:1 complexes with cholesterol. Furthermore, in *Escherichia coli* it has been shown that endogenously produced NAPEs, together with phosphatidic acid, are significantly enriched at the cell poles and division site domains, meaning that NAPEs may organize amphitropic cell division proteins at specific sites on the membrane surface[7].

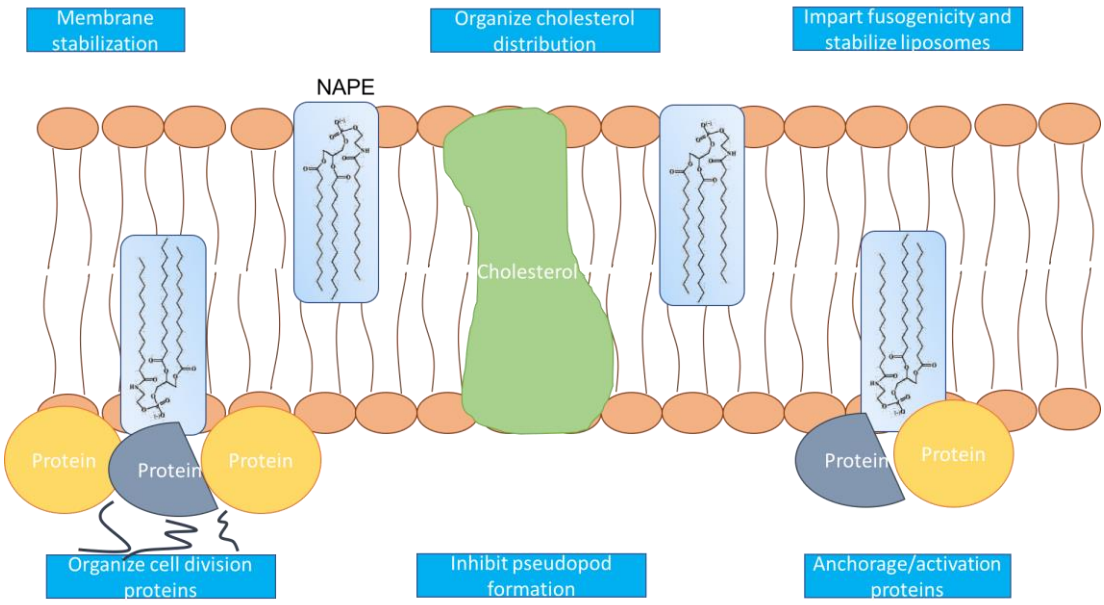

Figure 3: Hypothetical NAPEs functions. *NAPEs may be involved in membrane stabilization and organization; they interact with intracellular proteins, stabilizing their anchorage to the membrane or stimulating their activity; they are involved in the organization of cell division pole at the membrane, and inhibits pseudopod formation.*

Furthermore, NAPEs can block phagocytosis in macrophages, probably via inhibition of pseudopodia formation[32].

In addition, these lipids are interesting molecules in lipid based formulation for drug delivery[17]. Indeed, NAPEs can stabilize the lipid bilayer in liposomes preventing liposome leakage, or they can modify the permeability and impart fusogenicity to vesicles in a divalent cation dependent manner[6]. Specifically, in the presence of divalent cations NAPEs can flip in the membrane, inducing a deep insertion of the N-linked acyl chain in the bilayer that leads to a negative curvature of the membrane that facilitates fusion[6].

1.5 NAPEs in neurodegeneration

NAPE levels strongly increase in response to stress conditions involving degenerative membrane changes. Thus, during myocardial ischemia significantly higher levels of NAPEs (mainly N-palmitoyl-PE and N-stearoyl-PE) were detected for the first time in dog heart[33]. Furthermore, increases in *in vivo* NAPE levels were reported in inflamed rat testis[34] and in the uterus of pregnant mice[35].

NAPE production in the nervous system has been widely studied: NAPEs are increased in the brain following injurious stimuli of diverse nature. For instance, following post-decapitative ischemia, NAPE levels reach 1.5% of total phospholipids in the brain of young rats[8,36]. Many papers report that NAPE synthesis can also be triggered by the presence of toxic molecules. For example, in cultured neocortical neurons, sodium azide (mitochondrial respiratory chain inhibitor) induced an increase in NAPE levels that might be related to neuronal death[10]. The same effect has been observed in cultured cortical neurons when treated with glutamate[11,37] and hydrogen peroxide. *In vivo,* neuronal death induced by ischemia[36,38,39], by excitotoxicity (kainate and NMDA administration)[9], or by high doses of ethanol[12] resulted in increased formation of NAPEs. Moreover, neuronal tissue from all investigated species has a large capacity for NAPEs production during injury-induced calcium influx[37,40].

The accumulation of many species of NAPEs is generally restricted to area of neuronal cell death, as recently demonstrated using mass spectrometry imaging technique[39]. This phenomenon may be explained by the remarkable increase in intracellular Ca^{2+} concentration, which results in the activation of Ca-NAT. In support to this theory, also physiologically relevant Ca^{2+} spikes were reported to stimulate NAPE production in intact neurons[20,41]. It is still not clear whether PLA/AT-1 is involved in NAPE formation during cardiac infarction, brain ischemia, testicular

inflammation or during physiological increases in intracellular Ca^{2+}, given the fact that the enzyme activity of PLA/AT family is not enhanced by Ca^{2+} [16].

It is worth of notice that in neonatal rats exposed to neurotoxic stimuli, NAPE levels in the brain can increase up to 46-fold, while this is only 2-3 fold in adult rats[38]. This phenomenon can be explained by an opposite developmental change in the activities of NAT and NAPE-PLD: while NAT activity decreases during development, in adult age NAPE-PLD is more active[36].

Finally, we have recently developed a new method for the detection of low intensity lipid signals in complex tissue samples[13]. It consists in a combination of liquid chromatography/mass spectrometry and ion mobility mass spectrometry. This methodology lead us to observe that particular species of NAPEs are increased following the administration of the Parkinson's disease inducer 6-hydroxydopamine, in the Caudate Putamen of mice[13]. Even in this case, the increase in NAPE production was limited at the area of toxin administration, suggesting that these lipid molecules may be strictly related to the neurodegenerative process.

2. PARKINSON'S DISEASE

In his 1817 "An essay on the shaking palsy", James Parkinson first described the clinical syndrome that was later to bear his name[42]. Charcot, later in the 19th century, gave credit to Parkinson by referring to this disease as "maladie de Parkinson" or Parkinson's Disease (PD). More than 100 years passed (1925) before the neuropathological hallmarks underlying the clinical phenotypes were elucidated as the loss of dopaminergic neurons in the substantia nigra, together with the presence of intraneuronal inclusions termed Lewy bodies. 140 years after the original description by Parkinson (1957), dopamine was discovered as a putative neurotransmitter by Carlsson and colleagues[43]. The subsequent discovery by Ehringer and Hornykiewicz in 1960 that dopamine concentrations are remarkably decreased in the striatum of patients with PD paved the way for the first trials of levodopa in PD patients the following year and subsequent award of the Nobel Prize in Medicine to Carlsson (Kandel and Greengard) in 2000[44].

PD is a chronic progressive neurodegenerative disorder characterized by the presence of motor symptomatology (bradykinesia, rigidity, rest tremor and postural disturbances)[45], accompanied by an assortment of non-motor symptoms such as hyposmia, sleep behavior disorder, rapid eye movements, pain, personality

changes, paresthesias and depression, that may even manifest before the motor symptoms.

The prevalence of PD in industrialized countries is estimated at 0.3% of the entire population and about 1% in people over 60 years of age[46]. Reported standardized incidence rates of PD are 14 per 100,000 people in the total population, and 160 per 100,000 people aged 65 years or older[46]. PD usually initiates in the fifth or sixth decade of life, but a small number of patients develop the disease at early age. PD is primarily sporadic, meaning that it arises in the absence of any obvious genetic linkage. However, in rare instances, PD is inherited and the phenotype is transmitted either as a recessive or dominant trait[47]. Yet the motor phenotypes of both the sporadic and familial forms of PD are almost identical, implying that they might share common underlying mechanisms.

The pathological hallmarks of PD are the loss of the nigrostriatal dopaminergic neurons and the presence of intraneuronal proteinaceous cytoplasmic inclusions termed Lewy Bodies, accompanied by microgliosis. Lewy bodies are mainly composed by α-synuclein and other misfolded proteins. The cell bodies of nigrostriatal neurons are located in the substantia nigra pars compacta (SNpc) and they project primarily to the caudate putamen (CPu). The SNpc neurons form the nigrostriatal dopaminergic circuit, which controls voluntary movements via the release of dopamine by these cells. Depletion of dopamine is most pronounced in the dorsolateral putamen, the main site of projection for these neurons. At the onset of the symptoms, putamenal dopamine is depleted ~80%, and ~60% of SNpc dopaminergic neurons have already been lost. The fact that the degree of terminal loss in the striatum is more conspicuous than the SNpc dopaminergic neuron loss, suggests that striatal dopaminergic nerve terminals are the primary target of the degenerative process and that neuronal death in PD may result from a “dying back” process[47]. The consequence of this denervation process is an imbalance in the striato-pallidal and pallido-thalamic output pathways, leading to an impairment in the initiation and the execution of movement (Fig. 4).

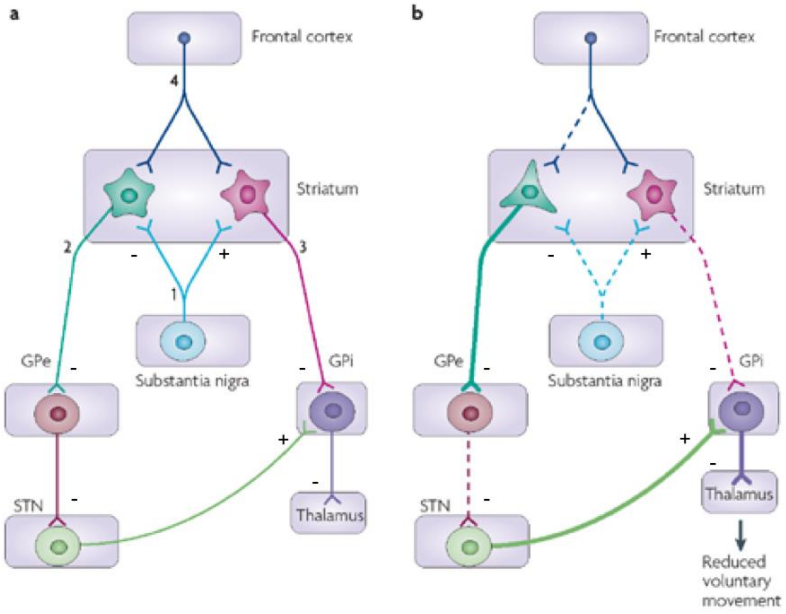

Figure 4: Classical model of the basal ganglia changes that underlie Parkinson's Disease. a) *Interconnections in the healthy condition. Dopaminergic input from the nigrostriatal pathway (1) synapses act on the striatal output neurons that mediate the indirect and direct GABA (gamma-aminobutyric acid)-ergic output pathways. The indirect pathway (2) has inhibitory D2 dopaminergic receptors on its cell bodies, whereas the direct output pathway (3) has excitatory D1 dopaminergic receptors on its surface. The indirect (inhibitory) output pathway projects to the external globus pallidus (GPe), where it synapses on to the GABAergic pathway that projects to the subthalamic nucleus (STN). The glutamatergic neurons of the STN project to the internal globus pallidus (GPi), where they synapse on to GABAergic output to the thalamus. The direct (excitatory) output pathway projects to the GPi, where it synapses on to GABAergic output to the thalamus. Another input to the striatum comes from the frontal cortex (4).* ***b)*** *According to classical thinking about Parkinson's disease, loss of dopaminergic input from the substantia nigra leads to overactivity of the indirect (inhibitory) output pathway and underactivity of the direct (excitatory) output pathway. The number of dendritic spines on medium spiny neurons in the striatum is reduced. Cortical glutamatergic input to the striatum is also altered.*

PD is considered a multi-factorial disorder with both genetic defects and environmental factors influencing disease progression. Only 10% of all cases are linked to a genetic cause. To date 16 PARK loci have been reported, with synuclein-α (SNCA, PARK1/4), LRRK2 (PARK8), *parkin* (PARK2) and PINK1 (PARK6) as the most common causes of familial PD. In addition, mutation in SNCA, LRRK2 and *parkin* have also been reported in sporadic PD[48]. Animal models of the disease support a critical interaction between genetics and the environment in PD pathogenesis. Indeed, the alterations in protein processing, with α-synuclein as the main culprit, and the mitochondrial dysfunction together with increased formation of reactive oxygen species, are a probable biological mechanism contributing to dopaminergic neuron loss[49]. A substantial body of evidence also suggests that, in addition to or intermingled with these mechanisms, neuroinflammation may contribute to neuronal damage[50]. All these mechanisms are present both in familial and in sporadic PD, supporting a multi-factorial etiology.

To date no therapies have been developed to cure PD: current treatments are symptomatic, but they do not stop the neurodegenerative process. The gold standard treatment is the administration of the dopamine precursor L-DOPA, dopamine agonist and/or dopamine degradation blockers. However the relief provided by this therapy is impaired in the long-term by loss of efficacy and the appearance of dose-dependent side effects: L-DOPA-induced dyskinesia and motor fluctuations[51]. Since the middle of the 1990s, deep brain stimulation has become a successful and frequently practiced neurosurgical approach for alleviating PD motor symptoms, in particular, stimulation of the subthalamic nucleus at high frequency. However, the fact that a pharmacotherapy first used in 1960s remains the front-line treatment choice for PD, underscores our lack of knowledge about the causes of neuronal degeneration in this disease.

2.1 Molecular pathogenesis of Parkinson's disease

Whatever insult initially raises neurodegeneration, studies on toxic and genetic PD models proposed several pathogenic processes that might contribute to dopaminergic neuron loss in PD (Fig. 5). They include oxidative stress, mitochondrial dysfunction, impaired of calcium homeostasis, altered endoplasmic reticulum to Golgi trafficking, and altered mitophagy and proteasome function, among others. These factors are not mutually exclusive.

The earliest hypothesis of PD pathogenesis was based on the discovery that three different mitochondrial complex 1 inhibitors, MPTP, rotenone and paraquat can emulate parkinsonism, leading to a selective loss of dopaminergic neuron *in vitro* as well as *in vivo*[47]. Inhibition of complex 1 causes ATP depletion, leading to an impairment of all ATP-dependent cellular processes, and production of free radicals that cause oxidative stress. Mitochondrial defects and oxidative stress are strictly correlated. Indeed, every condition that impairs mitochondrial function enhances radical oxygen species (ROS) formation and vice versa. In particular, the SNpc is exposed to high rates of ROS generation, because of the great abundance of cytoplasmic dopamine, which is prone to autoxidation, accompanied by a high iron content typical of this nucleus[52]. These conditions create an adverse environment for mitochondria, whose density and mass are lower in SNpc neurons[53]. The massive oxidative catabolism of dopamine can impair mitochondrial respiration and membrane permeability. Moreover, dopamine can modify several chaperones involved in mitochondrial protein quality control[54]. Thus, dopamine may be pivotal in rendering SNpc dopaminergic neurons particularly vulnerable to oxidative attack.

Further support for primary role of oxidative stress and mitochondrial dysfunction, has emerged from the study of genetics of PD: virtually all proteins involved in genetic PD are associated with mitochondria, although with different functional roles. For instance, LRRK2 and α-synuclein have been found to be associated with the mitochondria outer membrane. DJ-1 (PARK7) is a cytosolic protein that acts as an oxidative stress sensor and translocates to mitochondria under oxidative conditions. PINK1 can localize to both mitochondria and cytoplasm. Parkin is an ubiquitin ligase, which can translocate to mitochondria after phosphorylation by PINK1, acting as a mitochondria quality control pathway[55].

Another player in the pathogenesis of PD is the abnormal accumulation and processing of mutant or damaged proteins. Under physiological conditions, abnormal or misfolded proteins are normally targeted via ubiquitination to the proteasome or directed to the autophagic-lysosomal pathway. PD pathology is characterized either by the production of mutated and possibly toxic protein conformations, resulting in intracellular aggregation, or by alteration of the processes that normally recognize and process misfolded proteins, with subsequent accumulation and aggregation of cytotoxic damaged proteins, determining neuronal death.

α-Synuclein is a synaptic vesicle protein located in the cytoplasm or within lipid membranes, implicated in neurotransmitter release, synaptic plasticity, vesicle turnover and endoplasmic reticulum trafficking[56]. This protein is often overexpressed and misfolded in PD, leading to accumulation and aggregation to form Lewy bodies in the cytosol. Moreover, aggregated α-synuclein can inhibit proteasome function interfering with the ubiquitin-proteasome system[57]. At the same time, the presence of ROS would increase the amount of misfolded proteins, boosting the demand of the ubiquitin-proteasome system to remove them.

The mitochondrial system and the ubiquitin-proteasome system (UPS) are interconnected: complex 1 inhibitors cause a reduction in proteasomal activity[58], and conversely, proteasomal inhibitors can cause mitochondrial damage. There is also evidence for a relationship between mitochondrial dysfunction and protein aggregation: complex 1 inhibition and other forms of oxidative stress lead to α-synuclein aggregation[59].

A third, common feature of PD is endoplasmic reticulum (ER) stress. Recent reports place ER dysfunction as an early player of PD pathogenesis[60]. The homeostasis of the ER can be altered by diverse conditions including calcium depletion from its

lumen, oxidative stress and mutation in proteins that traffic through the secretory pathway, among other events. All of these perturbations can result in disruptions of the folding process in the ER, leading to the accumulation of misfolded/unfolded proteins (ER stress). ER stress activates the unfolded proteins response (UPR), a complex signal-transduction pathway that mediates cellular adaptation to restore ER homeostasis. Under chronic ER stress the UPR triggers cell death by apoptosis, eliminating damaged cells. Moreover, ER stress, induced by alterations in calcium levels, or other factors, may feed-back to enhance α-synuclein aggregation[61], suggesting a vicious cycle between ER stress and α-synuclein aggregation. Thus, the ER may represent the possible site of formation and accumulation of α-synuclein neurotoxic species, which may sequester important ER chaperones, leading to impaired ER folding and chronic stress. Furthermore, impaired vesicle transport from the ER triggers the accumulation of immature proteins in this compartment, and ER-Golgi trafficking defects were also shown to affect mitochondrial functioning[60].

Finally, it is now well accepted that chronic neuroinflammation is a pathological feature of the Parkinson's disease[50]. Inflammatory processes, which normally prompt tissue protection and repair, might become detrimental and amplify cell death in a stressed or intoxicated microenvironment, such as the PD brain. They may contribute to oxidative damage to the nigrostriatal system; this is related to the massive release of nitric oxide, and subsequent formation of reactive nitrogen species, due to activation of inducible nitric oxide synthase, which is a typical phenomenon associated with microglia activation[62]. However, neuroinflammation does not seem to be the primary cause of cell death, but rather, it may be a secondary event that perpetuates the vicious cycle of neurotoxicity[63].

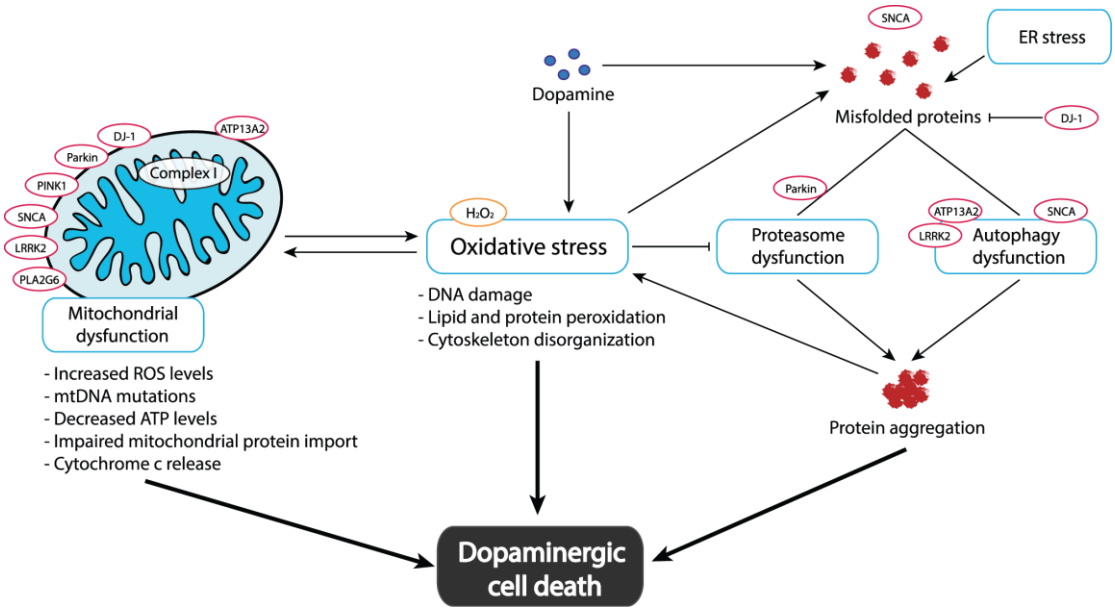

***Figure 5: Molecular mechanism dysregulated in PD**. Mitochondrial, proteasomal and autophagy dysfunction, protein aggregation, dopamine meabolism and oxidative stress, partecipate to determine dopaminergic neurons death.*

To summarize, there are multiple levels of intersection between these pathways (Fig. 5) rather than a minor abnormality in one or more cellular processes. Thus, the alteration of one pathway can be amplified by its interaction with other cellular processes to potentially result in several forms of stress that would ultimately force a cell into programmed cell death. Hence, many factors implicated in the pathogenesis of PD may converge to generate a proteotoxic insult to cells.

2.2 Experimental models of Parkinson's disease

Animal models of PD can be classified in three main categories:

1. "classic" models based on neurotoxins that selectively target catecholaminergic neurons (such as 6-hydroxydopamine, 1-methyl-1,2,3,6-tetrahydropiridine, agricultural pesticides etc.);
2. more recent models employing genetic manipulations that either introduce similar mutations to those find in familial cases of PD (α-synuclein, DJ-1, Parkin etc.);
3. genetic models that selectively disrupt nigrostriatal neurons (MitoPark, Pitx3, Nurr1, etc.).

Each one of these models has its own advantages and limitations, thus some are better suited for studying PD pathogenesis, while others are more appropriate to test potential therapeutic treatments. None of the current available models phenocopy

PD, mainly because they lack some specific neuropathological and/or behavioral feature of this disease[47].

The crucial requirement for an etiologic model of PD is the adult onset of relatively specific and progressive dopaminergic neuron degeneration. A behavioral correlate of the nigrostriatal dopaminergic pathway degeneration is also desirable, but rodents do not develop typical parkinsonism because motor system organization differs between rodents and humans. Thus, the value of a specific behavioral phenotype depends upon its relationship to striatal dopaminergic function rather than apparent similarity to a symptom of PD. The formation of Lewy bodies is also a desirable but not essential feature. Lewy bodies are not a specific characteristic of PD, indeed, they are not found in a minority of clinically defined PD cases, such as *parkin*-related PD.

It is important not just using any model but in selecting the optimal model whose strengths are appropriate for investigating the question being asked and whose weaknesses will not invalidate the interpretation of an experiment.

2.2.1 Gene-based models

The rationale for investigating rare genetic forms of a common sporadic illness is the expectation of a phenotypic similarity between the genetic and sporadic forms of the disease, indicating common pathogenic mechanisms and, help in the research on a key biochemical pathway.

The most common genetic PD models are SNCA (α-synuclein, PARK1 and 4), *parkin* (RBR E3 ubiquitin protein ligase, PARK2), PINK1 (PTEN-induced putative kinase 1, PARK6), DJ-1 (PARK7) and LRRK2 (leucine-rich repeat kinase 2, PARK8). All these models show little or no nigrostriatal degeneration, striatal dopamine depletion and motor symptoms. Only some of these models develop α-synuclein aggregates in the SNpc and other brain regions. In general, these models offer the possibility to study the pathology and pathogenesis of PD, and to better understand the role of these proteins in both physiological and pathological states.

Inactivation of multiple PD genes is insufficient to cause significant nigral degeneration. Thus, other approaches have been used to create new models, based on the deletion of transcription factors necessary for the development and survival of dopaminergic neurons, such as sonic hedgehog (SHH), pituitary homeobox 3 (Pitx3), nuclear receptor related protein-1 (Nurr1), engrailed 1 (EN1). These mice showed loss of dopaminergic neurons without Lewy bodies formation

and altered locomotor activity. The “MitoPark” model is based on the inactivation of a mitochondrial transcription factor selectively in dopaminergic neurons, resulting in a parkinsonism phenotype that includes an adult-onset, slowly progressive impairment of motor function, dopaminergic neuron death, intraneuronal inclusions and degeneration of nigrostriatal pathways[64]. Overall, these models can be appropriate for addressing neuroprotection[65].

2.2.2 Toxin-based models

Neurotoxin-based models can induce massive degeneration of the nigrostriatal pathway that produces strong motor symptoms. These models have been widely used to elucidate the neurodegenerative process of SNpc dopaminergic neurons and to test symptomatic treatments. Among the neurotoxins used to cause dopaminergic neurodegeneration, 1-methyl 4-phenyl 1,2,3,6-tetrahydro-pyridine (MPTP), 6-hydroxydopamine (6-OHDA), and more recently rotenone, paraquat and maneb have received attention.

- The neurotoxic power of MPTP was discovered in 1982, when young drug-addicted Californians injected with synthetic heroin accidentally contaminated with MPTP, and suddenly developed parkinsonian symptoms. In humans, monkeys and mice, MPTP produces an irreversible and severe parkinsonian syndrome. A weakness of this model is the lack of Lewy bodies. Indeed, only MPTP-injected monkeys have intraneuronal inclusions, reminiscent of Lewy bodies.

  After systemic administration, MPTP, which is highly lipophilic, crosses the blood-brain barrier within minutes. Once in the brain, the pro-toxin MPTP is oxidized to 1-methyl-4-phenyl-2,3-dihydropyridinium (MPDP+) by monoamine oxidase B in glia and serotoninergic neurons, the only cells that contain this enzyme. It is then transformed to MPP+ (probably by spontaneous oxidation), the active toxic molecule, and released into the extracellular space. MPP+ is a high-affinity substrate for the DAT, as well as for norepinephrine and serotonin transporters[66]. Once inside neurons, MPP+ accumulates in the cytoplasm and into synaptic vesicles. MPP+ also enters the mitochondria and impairs oxidative phosphorylation by blocking the multienzyme complex I of the mitochondrial electron transport chain[67]. This blockade rapidly leads to decreases in tissue ATP content, leading to the up-regulation of the apoptosis regulator Bax and the kinase JNK, accompanied by the release of cytochrome c and the activation of caspase-3 and 9, as well

as NMDA receptor-mediated excitotoxicity and neuroinflammatory processes[68]. Furthermore, by hindering the flow of electrons through complex I, MPP+ can stimulate the production of ROS, especially superoxide.

- Rotenone is a widely used herbicide, pesticide and piscicide. Interestingly, it reproduces almost all PD hallmarks. Indeed, the administration of low-dose intravenous rotenone to rats induces SNpc dopaminergic neuron loss, nigrostriatal dopaminergic denervation, behavioral alterations, inflammation, Lewy bodies-like inclusions containing α-synuclein and ubiquitin, oxidative stress and gastro-intestinal problems[69].

  Highly lipophilic, rotenone easily crosses the blood brain barrier and enters all cells without being dependent on a specific transporter. Its mechanism of action includes binding and inhibition of mitochondrial complex I (at the same site as MPP+), with subsequent production of intracellular ROS. It is also able to block proteasome activity and decrease dopamine and GSH levels, resulting in oxidative damage.

- Paraquat (N,N'-dimethyl-4-4'-bipyridinium), a widely used pesticide and herbicide was identified as an environmental contaminant with a molecular similarity to MPP+. Exposure to paraquat may confer an increased risk for PD. Indeed, systemic chronic administration of paraquat to mice leads to a slowly progressive SNpc dopaminergic neuron degeneration accompanied by α-synuclein containing inclusions[59].

  Paraquat does not easily penetrate the blood brain barrier[70] and it is not a good substrate for the dopamine transporter. Toxicity induced by paraquat is primarily mediated by redox cycling with cellular diaphorases such as NADPH oxidase and nitric oxide synthase, stimulating the generation of superoxide[71]. In addition, the action of this toxin seems to induce the sequential phosphorylation of JNK and c-Jun, and the activation of caspase-3, leading to apoptosis[68].

- Maneb has been shown to potentiate the effects of both MPTP[72] and paraquat. One of the advantages of using paraquat and/or maneb model relies on their ability to induce the expression of Lewy bodies-like inclusions containing α-synuclein[59].

- 6-hydroxydopamine will be discussed in the next paragraph.

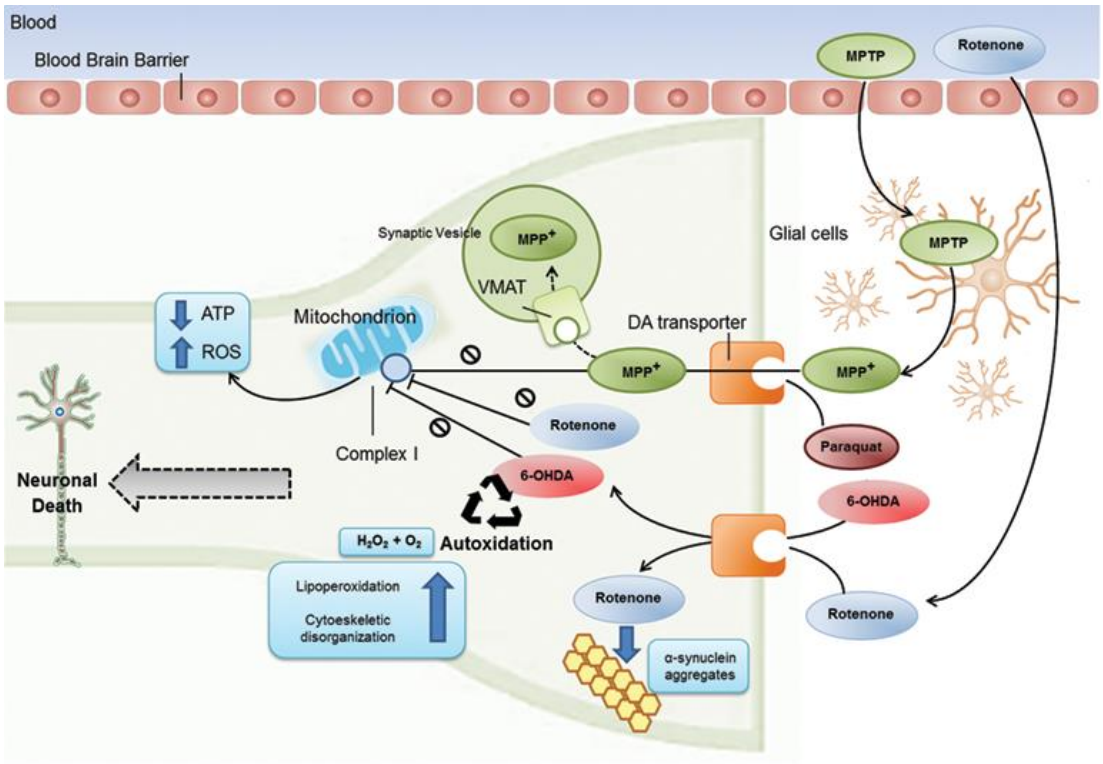

Figure 6: Pathogenesis of toxin-induced models. *MPTP crosses the blood-brain barrier and is metabolized to 1-methyl-4-phenylpyridinium (MPP+), the active toxic compound, by the enzyme monoamine oxidase B (MAO-B). MPP+ is then internalized by dopamine transporter and enters dopaminergic cells, where it impairs mitochondrial respiration by inhibiting complex I of the electron transport chain, leading to oxidative stress and activation of programmed cell death pathways. Both paraquat and 6-hydroxydopamine (6-OHDA) easily cross cell membrane through the dopamine transporter and exert their toxicities, in part, by damaging mitochondria with the subsequent production of ROS and quinones causing the degeneration of the nigrostriatal dopaminergic neurons. Rotenone is extremely hydrophobic and penetrates easily the blood brain barrier and cellular membrane inducing the formation of α-synuclein aggregates and mitochondrial impairment followed by ROS and quinones production.*

2.2.3 6-Hydroxydopamine

6-Hydroxydopamine (6-OHDA), the first neurotoxin associated with SNpc dopaminergic neuronal death, was introduced in PD research almost 50 years ago[73]. 6-OHDA induced-toxicity is relatively selective for monoaminergic neurons, resulting from preferential uptake by dopaminergic and noradrenergic transporters. The neurotoxicity of 6-OHDA is mainly imputed to its ability to form ROS that may arise from two distinct mechanisms: deamination by monoamine oxidase or auto-oxidation.

Indeed, 6-OHDA, like DA, is a substrate for monoamine oxidase (MAO) and this enzymatic reaction produces hydrogen peroxide. Accordingly, selegiline, a MAO inhibitor, prevents 6-OHDA toxicity. However, several lines of evidence suggest that under physiological conditions, 6-OHDA undergoes a rapid and nonenzymatic auto-oxidation[74], shown to generate several toxic species including quinones, hydrogen peroxide, superoxide radicals, and the highly reactive hydroxyl radical. The

formation of ROS generated either by MAO or autoxidation may be amplified by iron that catalyzes a Fenton reaction. Indeed, iron levels are elevated in SNpc and striatum after 6-hydroxydopamine injection. The participation of iron in 6-OHDA toxicity is also suggested by studies showing that 6-OHDA-induced neurotoxicity is prevented by iron chelating agents[75] and that direct administration of iron into the SNpc produces similar neurotoxic effects.

Oxidative stress impairs intracellular redox potential regulation and causes lipid peroxidation accompanied by DNA strand break, mutations, impairment of glucose uptake and a disorganization of the cytoskeleton. 6-OHDA can also impair mitochondrial function by various mechanisms: first of all, it interacts with and inhibits complex I in isolated brain mitochondria[76], independently from ROS formation. Moreover, 6-OHDA stimulates a ROS-related collapse in mitochondrial membrane potential and is a strong uncoupler of oxidative phosphorylation. As a result of these toxic events, both necrotic and apoptotic mechanism of cell death occur in response to 6-OHDA[77].

Because 6-OHDA cannot cross the blood brain barrier, it must be administered by local stereotaxic injection into the SNpc, median forebrain bundle (MFB) or striatum, destroying nigral dopaminergic neurons and depleting the pool of dopamine in the striatum.

Although generally nerve terminals are more sensitive to 6-OHDA toxicity than axons and cell bodies, when injected into the SNpc or in the MFB, 6-OHDA produces a massive (>90%) and extremely rapid lesion in the nigrostriatal pathway[78]. Indeed, substantia nigra injections induce degeneration of dopaminergic neurons within 12 hours, preceding a significant loss of striatal terminals, that occurs 2-3 days later[78]. The injection in the MFB, induces degeneration in striatal terminals before dopaminergic cell death occurs[79].

In contrast to the nigra and MFB, when delivered into the striatum, 6-OHDA induces slow, progressive and partial damage to the nigrostriatal structure (~60%) in a retrograde fashion over a period of up to 3 weeks[80]. In particular, following striatal administration of 6-OHDA, the loss of dopaminergic fibers in the striatum begin immediately and is very rapid: one day after 6-OHDA administration, 60% of dopaminergic fibers are already degenerated, remaining stable later on. Despite the rapid loss of axonal fibers in the caudate, changes in the SNpc neurons are not immediately appreciable. Indeed, alterations in cell size, dendrite length and gene expression require several days, and the reduction in the number of dopaminergic

cells is not significant until 6-9 days post-surgery. The apoptotic cascade is activated from 9 days post-lesion and condensed chromatin is observed in dying dopaminergic neurons at 12 days post-surgery. Moreover, ROS are highly diffusible through biological membranes and suitable for cellular signaling, recruiting microglial cells and astrocytes. 6-OHDA induces a pronounced progressive microgliosis and astrogliosis in the caudate at early stages post-lesion; on the other hand, in the SNpc the activation and proliferation of microglia and astrocytes does not occur until 6-9 days post-surgery, with a slight advance of microgliosis[81].

For striatal stereotaxic lesions, 6-OHDA is generally injected unilaterally for two main reasons: first of all, each animal can serve as its own control, with a lesioned and unlesioned hemisphere; second, bilateral lesions are reported to cause aphagia and adipsia. However, the major advantage of using the 6-OHDA model is its rather unique effect on quantifiable circling motor abnormality in animals[82]: subsequent to the unilateral lesioning, systemic administration of dopamine receptor agonists, or dopamine releasing compounds induces asymmetrical rotation[82]. Importantly, magnitude of nigrostriatal lesions correlates with the circling motor behavior[80,82].

Bilateral lesions in the CPu would probably serve as a closer parallel to the human disease than unilateral lesions because both striata are affected in human PD. However, a notable advantage of this model is the ability to assess the anti-PD properties of new drugs and the benefit of transplantation or gene therapy to repair the damaged pathways. Furthermore, the fact that the administration of 6-OHDA in the striatum leads to a gradual loss of dopaminergic neurons, gives the opportunity to study early phases of the pathology and use this therapeutic window to investigate potential neuroprotective effectors. On the other hand, 6-OHDA model lacks the progressive age dependent effects of PD and do not show formation of Lewy bodies.

2.2.4 Basic assessments of the nigrostriatal dopaminergic structure and function

To evaluate neurodegeneration or neuroprotection using neurotoxic models, the most common assessment is to analyze the integrity and function of the nigrostriatal pathway. For this purpose, some specific techniques have been developed over the years. In the chapter below, I will summarize the most used techniques and the ones I used during my work.

Quantification of dopaminergic neurons in the SNpc: in the mesencephalon, there are three groups of dopaminergic neurons classified historically as A8, A9 and

A10. The A8 group is located in the retrorubral area, whereas the A9 and A10 groups belong to the substantia nigra and ventral tegmental area, respectively. The distribution of dopaminergic neurons in the nigra is not homogeneous. Thus, when the nigra is sectioned coronally, there is a great difference in the density of dopaminergic neurons between the caudal and the rostral regions. It is necessary, therefore, to sample the population of dopaminergic neurons at different levels throughout the entire SNpc. One way to sample the entire area efficiently is to count dopaminergic neurons systematically at a regular section interval. For this purpose, the gold standard is to use an unbiased stereological cell counting with optical dissector system[83]. Major components required for this method are computerized stereology software and a microscope with a motorized stage.

Quantification of dopaminergic terminals in the striatum: the projection of fibers to the striatum from the nigral dopaminergic neurons has been well established[84]. Although the density of striatal dopaminergic terminals frequently correlates with number of their cell bodies in the SNpc, it is not uncommon to observe differential damage or protection between these two structures. Indeed, striatal fibers are more sensitive to 6-OHDA toxicity than cell bodies and the quantification of striatal dopaminergic terminals is also informative of neurodegeneration. The density of striatal dopaminergic terminals can be digitized and then quantified based on optical density of fiber density of tyrosine hydroxylase immunoreactivity. As an alternative to immunostaining, fresh striatal tissue can be isolated for immunoblotting using tyrosine hydroxylase or dopamine transporter as markers to assess the entity of the lesion[83].

Quantification of dopamine content in the striatum: in addition to structural analysis, it is also important to assess the function of the nigrostriatal pathway. A common way to measure dopamine is to use reverse-phase high-performance liquid chromatography (HPLC) coupled with electrochemical detecting[83].

Assessment of motor function: many behavioral tests are designed to assess motor phenotypes linked to the nigrostriatal function such as locomotor activity, rotation, rotarod, stride length of the paws, cylinder test and pole test[85].

In many cases, animals with unilateral lesion present characteristic features when given a choice: they (I) spontaneously prefer food presented from ipsilateral side, (II) show more foot-slips and falls when traversing narrow beam or grids, (III) show reduced use of the contralateral paw for stabilization and balance when rearing, (IV) are much more likely to turn in the ipsilateral direction when confronting an obstacle,

and (V) show impaired stepping and placing reflexes when moved into whisker or paw contact with surfaces or edges. Many of these aspects have been formalized into standardized tests such as the cylinder and footprint tests.

1. LOCOMOTOR ACTIVITY: animal's movements around an open arena are observed and recorded. When placed in the center of a field, a mouse will typically run to the perimeter and then explore the whole arena remaining close to the wall (thigmotaxis). Over time, as the animal habituates to the environment, it will increase its movement through the central area before going back to the perimeter. This behavioral profile is the basis of the study of the open-field locomotor activity. Unfortunately, in rodents the motor component in this test is typically confounded by anxiety levels.
2. ROTATION TEST: this test has been used for decades to assess the motor asymmetry in the unilateral 6-OHDA injection[86]. Indeed, following unilateral dopamine depletion, the contralateral dopaminergic pathway remains intact, and the animal exhibits a marked spontaneous postural bias to the side of the lesion; this can be amplified and transformed by pharmacological activation into a head-to-tail turning response. Stimulation of dopamine release from intact terminals by indirect agonists (such as amphetamine) enhances the spontaneous bias, causing ipsilateral rotations, whereas activation of supersensitive receptors on the denervated side by a direct agonist (for example apomorphine) drives vigorous contralateral rotation. The rate of rotation is easily quantified using an automated rotometer test apparatus.
3. ROTAROD: this test measures body coordination and balance. Briefly, a mouse is placed on a rod that can rotate at fixed or accelerating speed. The length of time the animal can maintain balance and keep walking on the rotating rod is recorded. Mice are tested on separate trials at a series of fixed speeds, or into a single trial by an accelerate version of the test. The accelerating test is quicker and more efficient, but it confounds motor coordination at different speeds with fatigue, whereas the fixed-speeds test provides separate data on each range of rotation speeds and is probably more sensitive.
4. FOOTPRINT TEST: this test is a valid way to measure abnormal movement, analogous to the shuffling gait in PD patients, and can be used to measure the stride length of the paws. Briefly, the fore and hind limbs of the mice are painted with different colors and the mouse is encouraged to walk in a

narrow corridor over absorbent paper. The footprint patterns are then analyzed for a range of measurements, including stride length, base width, overlap between fore and hind paws and paw and finger splay.

5. CYLINDER TEST: is a simple and efficient test of unilateral deficiency in voluntary forelimb use[85]. Mice are placed in a glass cylinder and filmed: mice with unilateral 6-OHDA lesions exhibit a reduction in the use of the contralateral paw when rearing to explore the environment. Paw usage can be determined by measuring the number of impaired forelimb wall contacts made with the contralateral paw, as a percentage of total contacts[86].
6. POLE TEST: it is another way to assess body coordination and balance. The mouse is placed facing upward on top of a vertical made of wood or wire-mesh. A normal mouse would grip the pole before turning through 180° and slowly climbing down to the base. The time that the animal takes to orient downward and the total time spent to descend to the base of the pole is recorded. Abnormalities in response can include climbing, falling or slipping down backwards[87].

2.2.5 Cellular models of Parkinson's disease

Most new experimental therapeutic strategies for PD are now first evaluated using simpler models that are easier to get than the animals. This approach leads to a reduction of the number of animal experiments needed, and permits to deeply study the molecular mechanism underling the pathology with simpler techniques.

The most used models consist in the use of cells cultures or organotypic cultures.

Organotypic cultures represent a recently developed technique based on the culture of parts or the whole organ. This approach combine features of cell culture and intact animals: neurons are more easily accessible for pharmacology, gene transfer and repeated imaging than inside the animal. At the same time, organotypic cultures avoid the deprivation of neurons natural environment, maintaining afferent and efferent connections. Usually, brain slices from post-natal rat or mouse pups are used, cultured either on coverslips or on membranes at the interface between medium and the air of the incubator[88].

On the other hand, cell cultures can be classified in two subgroups: primary cultures of neurons and immortalized cell lines.

The most prominent advantages of cell cultures are the easy access to genetic and pharmacological interventions, other than for imaging studies and various biochemical assays. Moreover, the use of cells gives the possibility to implement

high-throughput screening for drug candidates. Obviously, primary cell cultures are physiologically more relevant than immortalized cell lines, but they are difficult to maintain and, depending on the age of the source animals or the dissection accuracy, can introduce experimental variability.

Primary cultures of neurons from SNpc of patients and controls may be considered the most reliable models to unravel the molecular mechanisms underlying this disease. However, the inaccessibility and lack of proliferation of such neurons largely precludes their use.

Alternatively, primary mesencephalic cultures are typically prepared from mouse or rat embryos. They contain midbrain dopaminergic neurons cultured in the context of their physiological neighbors. As other neuronal cultures, neurons readily differentiate and form neurites and synapses. Even though these cultures are often referred to as primary dopaminergic neurons, TH positive neurons actually represent only 5-10% of the total population. This fact constitutes an invincible obstacle because significant changes that may occur in dopaminergic neurons are diluted or cancelled by changes in non-dopaminergic neurons. Moreover, there is more variability between cultures prepared on different days and gene transfer is more difficult than in immortalized cell lines[89].

An emerging new category of cell models of PD is represented by patient-derived induced pluripotent stem cells (iPSC) that can be differentiated into dopaminergic neurons (and other relevant cell types such as glia cells)[90].

Immortalized cell lines include:

- non-neuronal tumor cell lines such as pheochromocytoma (PC12) cells[77];
- neuronal human tumor cell lines (SH-SY5Y)[91];
- mouse neuroblastoma cell lines (Neuro-2a);
- cells hybrids obtained by the fusion of mice embryonic ventral mesencephalic and neuroblastoma cells (MN9D).

They all represent homogenous populations of continuously proliferating cells; this allows large-scale experiments with reproducible results in a variety of tests. Moreover, all these cells mimic many aspects of the dopaminergic neuron death observed in PD when treated by neurotoxins such as MPP+, 6-OHDA or rotenone. In the present chapter, I will explore more in deep SH-SY5Y cells biology, the cellular model I used during my work.

The neuroblastoma SH-SY5Y cell line provides an unlimited supply of cells of human origin with the similar biochemical characteristics of human dopaminergic

neurons. SH-SY5Y cells are a thrice cloned subline of SK-N-SH cells which were originally established from a bone marrow biopsy of a neuroblastoma patient with sympathetic adrenergic ganglial origin in the early 1970s. This cell line has been widely used as a model of neurons, because they show many biochemical and functional properties of neurons. Indeed, the initial characterization of the SH-SY5Y cell line showed moderate activity of dopamine-β-hydroxylases and negligible levels of choline acetyl-transferase, acetylcholinesterase and butyryl-cholinesterase, basal noradrenaline release and tyrosine hydroxylase activity. Tyrosine hydroxylase is the rate-limiting enzyme of the catecholamine synthesis pathway and converts tyrosine to L-dopa, the precursor of dopamine, which is converted to noradrenaline by dopamine-β-hydroxylase. Furthermore, SH-SY5Y cells express dopamine transporter (DAT), a protein expressed only in dopaminergic neurons within the central neuron system, that is a prerequisite for MPP+ and 6-OHDA incorporation into neurons. This is the reason why the SH-SY5Y cell line has been widely utilized to study mechanisms of neurotoxin action.

Apart from the dopaminergic phenotype, the ability of the selected cell line to reproduce the cellular abnormalities of PD is crucial for the validity of the model. One of the main hallmarks of PD is α-synuclein aggregation. To mimic this pathological feature, overexpression of WT α-synuclein or stable expression of one of its familial mutations has been successfully used in SH-SY5Y cells[92]. Furthermore, spontaneous α-synuclein aggregation has been reported in non-transfected SH-SY5Y cells[93]and this cell line is sensitive to extracellular α-synuclein-induced toxicity. Other PD-related problems, such as abnormal mitochondrial function, oxidative stress and autophagy or proteasomal dysfunction, have been reproduced in SH-SY5Y cells as well. These hallmarks can be triggered by the administration of specific drugs or, alternatively, by the knockdown of a gene corresponding to a familial PD-gene or expression of a familial PD-gene.

As this cell line is derived from immature neoplastic neural crest cells that exhibit properties of stem cells, SH-SY5Y cells are induced to differentiate upon treatment with a variety of agents, among all retinoic acid[94] or brain derived neurotrophic factor[95]. The SH-SY5Y cells can be differentiated in a more pronounced dopaminergic phenotype, however, some agents that induce differentiation also confer tolerance to SH-SY5Y cells, thus the role of toxicity or protection cannot be evaluated in these cells[91]. On the other hand, use of undifferentiated SH-SY5Y cells has some disadvantages. First, the number of cells increases during the experiment, so it is difficult to distinguish if an agent influence the proliferation rate or the rate of

cell death; second, SH-SY5Y cells in culture are unsynchronized and do not always express the typical markers of mature neurons. However, both undifferentiated and differentiated SH-SY5Y cells have gained broad acceptance as models of dopaminergic neurons, and they have been widely used as a PD cell model, even though both models show weaknesses.

To summarize, there are many other types of model besides the use of the animal, everyone has its advantages and weakness. It is important even in this case, to understand which is the best model to use, considering the aim of the study.

AIM OF THIS WORK

Parkinson's disease represents a huge burden for public health, with a predicted prevalence rate of 9 million people worldwide by 2030. Unfortunately, the etiology of neurodegenerative condition, is still poorly understood. Consequently, no therapy able to revert the pathology has been developed. Thus, there is the need to clarify molecular pathways that are involved in the neurodegenerative disease, to further develop new therapies to cure or prevent the progression of the pathology to late stage.

It is known that NAPEs are produced in large quantities in the injured brain.

The aim of the present work was to understand whether and how this process is involved in PD neurodegeneration.

To address these questions, I used a multidisciplinary approach, combining lipidomics, molecular and pharmacological techniques, using both *in vitro* and *in vivo* models of Parkinson's Disease.

MATERIALS AND METHODS

Chemicals

6-hydroxydopamine (6-OHDA) was purchased from Sigma Aldrich (Milan, Italy); solutions were prepared immediately before use in a vehicle consisting of 0.2% ascorbic acid in saline (0,9% NaCl).

ARN19874 was synthesized in our laboratory, the solution was freshly prepared in DMSO and used at a concentration of 50 μM.

Analytical grade standards of dopamine, serotonin, homovanillic acid (HVA) and 3, 4-dihydroxyphenylacetic acid (DOPAC) were purchased from Sigma Aldrich (Milan, Italy). NAPE standards and internal standards were synthetized in our laboratory as previous described[13].

Cells

SH-SY5Y cells were purchased from Sigma Aldrich (Milan, Italy) and cultured in Dulbecco's Modified Eagle's Medium (DMEM) (Euroclone, Milan, Italy) supplemented with 10% fetal bovine serum (FBS, Gibco, Thermo Fisher Scientific, Waltham, MA, USA), 2mM L-glutamine and antibiotics (Euroclone, Milan, Italy) at 37°C and 5% CO_2. Cells were treated with 100 μM 6-OHDA or vehicle (0.2% ascorbic acid saline) added to the culture medium, and analyzed at different time-points (2, 4, 6 and 8 h) post treatment. ARN19874 was administered to cells 2 h prior to 6-OHDA/vehicle, cells were then harvested and analyzed 8 hr post 6-OHDA administration.

Animals

C57BL/6J NAPE-PLD$^{-/-}$ mice were generated as described previously[28]. They were housed in a temperature and humidity controlled room under a 12 h light/dark cycle with water and food *ad libitum*. All procedures were performed in accordance with the Italian regulations on the protection of animals used for experimental and other scientific purposes (D.M. 116192), and European Union regulations (O.J. of E.C. L 358/1 12/18/1986). Mice were anesthetized with ketamine and xylazine (100 and 10 mg/kg, respectively, i.p.), placed in a stereotaxic frame and unilaterally lesioned in the striatum by two intracerebral injections (coordinates of the first and second injection respectively: anterior-posterior: +1 / +0.3; medial-lateral: +2.1 / +2.3; dorsal-ventral: -2.9). A small hole was drilled in the exposed skull and a cannula of

0.2 mm thickness (33 gauge) was used for administration of 6-OHDA (3.2 µg/µL; 1 µL each, at a rate of 0.25 µL/min). The cannula was left in place for 2 min before being slowly removed. Mice were then sutured and allowed to recover in a heated recovery chamber. Mice were sacrificed at different time-points (48h and 3 weeks) post-surgery and caudate putamen and substantia nigra were collected, snap-frozen in liquid nitrogen and stored in -80°C until analysis.

NAPE-PLD silencing and overexpression

Silencing. siRNA experiments were performed using the NAPE-PLD gene-specific 27mer siRNA duplex purchased from Origene Tecnologies (Rockville, MD, USA). siRNA duplex carrying TYE-563 fluorescence was used for transfection monitoring. siRNA duplex carrying a 27-mer sequence targeting HPRT gene was used as positive control. Scrambled siRNA were included in each experiment as control. NAPE-PLD siRNA complexes (10 nM) were formed by mixing siRNA with lipofectamine (Invitrogen, Thermo Fisher Scientific) for 10 min at room temperature and then added to SH-SY5Y cells cultured with 1% FBS Optimem medium (Gibco, Thermo Fisher Scientific). After 6 h, the medium was changed to fresh full growth medium, cells were further incubated for 18 h, then treated with 6-OHDA.

Overexpression. NAPE-PLD sequence was amplified from NAPE-PLD variant 2 cDNA (Openbiosystem, clone ID: 4375696) using the following primer pair: forward 5'-CGGGGTACCATGGATGAAAATGAAAGCAACC, and reverse 5'-ATAAGAATGCGGCCGCTTAAAAGTTTTCATCATCATTATTTAGG. The obtained sequence was cloned in the mammalian expression vector pCDNA3.1 (Life Technologies), using *KpnI* and *NotI* restriction enzymes. SH-SY5Y cells (1 x 10^6 cells/ plate) were transfected with NAPE-PLD construct using Jet Prime reagent (Polyplus transfectionTM, Illkrch, FR) following manufacturer's instructions. Briefly, plasmid (2 µg) was mixed with Jet Prime reagent (10 µL) and Jet Prime buffer (100 µL) for 15 min at room temperature and then added to the medium of SH-SY5Y cells. 24 h after transfection, cells were either analyzed for NAPE-PLD expression or treated with 6-OHDA.

Cell viability

To determine cell viability, SH-SY5Y cells were counted using a Scepter^{TM} cell counter (Merck Millipore, Darmstadt, DE). At the end of 6-OHDA incubation, the cells were harvested, diluted in PBS and counted. Cells with the same morphology and size were considered.

RNA isolation, cDNA synthesis and real time quantitative PCR

Total RNA was prepared using the Ambion purelink RNA mini-kit as directed by the supplier. Samples were treated with DNase to eliminate genomic DNA (PureLink DNase, LifeTecnologies, Milan, Italy) and cDNA synthesis was carried out with SuperScript VILO cDNA synthesis kit according to the protocol (LifeTecnologies) using 0.5-1µg of purified RNA. First-strand cDNA was amplified using the TaqMan Universal PCR Master Mix (LifeTechnologies) according to the manufacturer's instructions. Probes were purchased from Thermo Fisher Scientific. Quantitative PCR was performed in a 96-well PCR plate and run at 95°C for 10 min followed by 40 cycles, each cycle consisting of 15 sec at 95°C and 1 min at 60°C, using a ViiA7 instrument (ViiA™ 7 Real-Time PCR System, LifeTechnologies). To determine the expression stability and the geometric mean of different housekeeping genes (GAPDH, HMBS, HPRT) a free-available and widely used software (Bestkeeper, http://www.gene-quantification.de/bestkeeper.html[96]) was used. ΔCt values were calculated by subtracting the Ct value of the geometric mean of housekeeping genes from the Ct value for the genes of interest. The relative quantity of genes of interest was calculated by the equation $2^{-\Delta Ct}$. Data are reported as fold induction over control.

mRNA measurements by array

Substantia nigra specimens from the contralateral or ipsilateral side of three wild type mice and three NAPE-PLD$^{-/-}$ mice, were used for mRNA analysis. mRNA was extracted as reported above and cDNA synthesis was carried out with RT^2 First Strand Kit (Qiagen, Milan, Italy), according to manufacturer's instructions, using 0.25 µg of purified mRNA. First-strand cDNA was then load on the RT^2 Profiler PCR Array (Qiagen, Cod. 330231 PAMM-124ZA) and run at 95°C for 10 min followed by 40 cycles, each cycle consisting of 15 sec at 95°C and 1 min at 60°C, using a ViiA7 instrument (ViiA™ 7 Real-Time PCR System, LifeTechnologies). Data analysis was carried out with the SABiosciences PCR Array Data Analysis software (www.SABiosciences.com/pcrarraydataanalysis.php.), considering separately the two strain, with lesioned side versus control side. Genes analyzed are reported in Table 1.

Table 1: RT2 Profiler PCR Array genes

Position	Symbol	Description
A01	Aldh1a1	Aldehyde dehydrogenase family 1, subfamily A1
A02	Apc	Adenomatosis polyposis coli
A03	App	Amyloid beta (A4) precursor protein

A04	Atp2b2	ATPase, Ca++ transporting, plasma membrane 2
A05	Atxn2	Ataxin 2
A06	Atxn3	Ataxin 3
A07	Basp1	Brain abundant, membrane attached signal protein 1
A08	Bdnf	Brain derived neurotrophic factor
A09	Cadps	Ca2+-dependent secretion activator
A10	Casp1	Caspase 1
A11	Casp3	Caspase 3
A12	Casp7	Caspase 7
B01	Casp8	Caspase 8
B02	Casp9	Caspase 9
B03	Cdc27	Cell division cycle 27 homolog (*S. cerevisiae*)
B04	Cdc42	Cell division cycle 42 homolog (*S. cerevisiae*)
B05	Cdh8	Cadherin 8
B06	Chgb	Chromogranin B
B07	Cul2	Cullin 2
B08	Cxxc1	CXXC finger 1 (PHD domain)
B09	Ddc	Dopa decarboxylase
B10	Dlk1	Delta-like 1 homolog (*Drosophila*)
B11	Drd2	Dopamine receptor D2
B12	Egln1	EGL nine homolog 1 (*C. elegans*)
C01	Fbxo9	F-box protein 9
C02	Fgf13	Fibroblast growth factor 13
C03	Fn1	Fibronectin 1
C04	Gabbr2	Gamma-aminobutyric acid (GABA) B receptor, 2
C05	Gbe1	Glucan (1,4-alpha-), branching enzyme 1
C06	Gpr37	G protein-coupled receptor 37
C07	Gria3	Glutamate receptor, ionotropic, AMPA3 (alpha 3)
C08	Hspa4	Heat shock protein 4
C09	Htr2a	5-hydroxytryptamine (serotonin) receptor 2A
C10	Kcnj6	Potassium inwardly-rectifying channel, subfamily J, member 6
C11	Lrrk2	Leucine-rich repeat kinase 2
C12	Mapk9	Mitogen-activated protein kinase 9
D01	Mapt	Microtubule-associated protein tau
D02	Ncoa1	Nuclear receptor coactivator 1
D03	Nefl	Neurofilament, light polypeptide
D04	Nfasc	Neurofascin
D05	Nr4a2	Nuclear receptor subfamily 4, group A, member 2
D06	Nrxn3	Neurexin III
D07	Nsf	N-ethylmaleimide sensitive fusion protein
D08	Nsg1	Neuron specific gene family member 1
D09	Ntrk2	Neurotrophic tyrosine kinase, receptor, type 2
D10	Opa1	Optic atrophy 1 homolog (human)
D11	Pan2	PAN2 polyA specific ribonuclease subunit homolog (*S. cerevisiae*)
D12	Park2	Parkinson disease (autosomal recessive, juvenile) 2, parkin
E01	Park7	Parkinson disease (autosomal recessive, early onset) 7
E02	Pink1	PTEN induced putative kinase 1

E03	Ppid	Peptidylprolyl isomerase D (cyclophilin D)
E04	Prdx2	Peroxiredoxin 2
E05	Psen2	Presenilin 2
E06	Pten	Phosphatase and tensin homolog
E07	Rgs4	Regulator of G-protein signaling 4
E08	Rtn1	Reticulon 1
E09	S100b	S100 protein, beta polypeptide, neural
E10	Sept5	Septin 5
E11	Skp1a	S-phase kinase-associated protein 1A
E12	Slc18a2	Solute carrier family 18 (vesicular monoamine), member 2
F01	Slc25a4	Solute carrier family 25 (mitochondrial carrier, adenine nucleotide translocator), member 4
F02	Slc6a3	Solute carrier family 6 (neurotransmitter transporter, dopamine), member 3
F03	Slit1	Slit homolog 1 (*Drosophila*)
F04	Snca	Synuclein, alpha
F05	Spen	SPEN homolog, transcriptional regulator (*Drosophila*)
F06	Srsf7	Serine/arginine-rich splicing factor 7
F07	Stub1	STIP1 homology and U-Box containing protein 1
F08	Sv2b	Synaptic vesicle glycoprotein 2 b
F09	Syngr3	Synaptogyrin 3
F10	Syt1	Synaptotagmin I
F11	Syt11	Synaptotagmin XI
F12	Tcf7l2	Transcription factor 7-like 2, T-cell specific, HMG-box
G01	Th	Tyrosine hydroxylase
G02	Tpbg	Trophoblast glycoprotein
G03	Uba1	Ubiquitin-like modifier activating enzyme 1
G04	Ubc	Ubiquitin C
G05	Ube2i	Ubiquitin-conjugating enzyme E2I
G06	Ube2k	Ubiquitin-conjugating enzyme E2K (UBC1 homolog, yeast)
G07	Ube2l3	Ubiquitin-conjugating enzyme E2L 3
G08	Uchl1	Ubiquitin carboxy-terminal hydrolase L1
G09	Usp34	Ubiquitin specific peptidase 34
G10	Vamp1	Vesicle-associated membrane protein 1
G11	Vdac3	Voltage-dependent anion channel 3
G12	Ywhaz	Tyrosine 3-monooxygenase/tryptophan 5-monooxygenase activation protein, zeta polypeptide
H01	Actb	Actin, beta
H02	B2m	Beta-2 microglobulin
H03	Gapdh	Glyceraldehyde-3-phosphate dehydrogenase
H04	Gusb	Glucuronidase, beta
H05	Hsp90ab1	Heat shock protein 90 alpha (cytosolic), class B member 1
H06	MGDC	Mouse Genomic DNA Contamination
H07	RTC	Reverse Transcription Control
H08	RTC	Reverse Transcription Control
H09	RTC	Reverse Transcription Control
H10	PPC	Positive PCR Control
H11	PPC	Positive PCR Control

H12	PPC	Positive PCR Control

Western blot analyses

Proteins were obtained by lysis or omogenization of (10^6) cells or brain tissue (5-10 mg wet tissue) respectively, in RIPA buffer and quantified by BCA. Then 30 µg of protein were denatured in 8% SDS and 5% β-mercaptoethanol at 95°C for 5 min. After separation by SDS-PAGE on a 4-15% gel, or on a 3-8% Tris Acetate gel (for high weight proteins) under denaturing conditions, the proteins were electrotransferred to nitrocellulose membranes. The membranes were blocked with 5% non-fat dry milk in TBS and then incubated overnight with anti-NAPE-PLD (1:200, #ab95397, Abcam, UK), anti-LRRK2 (1:5000, #ab133474, Abcam, UK), anti-Rac1 (1:1000, #ab33186, Abcam, UK), anti-active Rac1 (1:1000, New East Biosciences, Malvern, USA), anti-FAK (1:1000, ZF002, Thermo Fisher, Rockford, USA), in 1% non-fat dry milk TBS containing 0.1% Tween-20, followed by incubation with horseradish peroxidase-linked anti-mouse or anti-rabbit IgG antibody (Millipore 1:5000 dilution) in TBS 0.1% Tween 20 at room temperature for 1 h. Finally, proteins were visualized using an ECL Kit (Bio-Rad, USA), and the chemiluminescence image was obtained using a LAS-4000 lumino-image analyzer system (Fujifilm, Tokyo, Japan). To control for protein loading, the membranes were then stripped and reprobed with a monoclonal antibody raised against GAPDH (1:2000, #ab9485, Abcam).

Lipid extraction and NAPE and FAE analysis

Tissue NAPE levels were quantified as previously described[13]. Briefly cell pellets were subjected to sonication and frozen caudate putamen were weighed (approximately 10 mg) and homogenized using a chloroform:methanol mixture (1:2 v/v, 2 ml) containing NAPE 18:0-22:6-17:1 and deuterated FAE (d4-OEA, d4-PEA and d3-SEA) as internal standards. After mixing for 30s, chloroform (0.6 mL) and water (0.6 mL) were sequentially added and vortexed after each addition. The samples were then centrifuged for 15 min at 3000xg at 4°C. After centrifugation, the aqueous (upper) and organic (lower) phase were separated by a protein disk. The organic phase was transferred to glass vials. For better extraction, the aqueous fraction was extracted again with chloroform (1 mL). Both the organic phases were pooled, dried under N_2. The organic extracts from brain tissues were suspended in chloroform (2 mL) and fractionated by silica gel column chromatography. NAPEs were eluted with chloroform/methanol (1:1, v/v). Organic phases were evaporated under nitrogen and reconstituted in 100 µL of methanol:chloroform (9:1, v/v). LC/MS

analyses were conducted on a Xevo TQ UPLC-MS/MS system (Waters) equipped with a reversed phase HSS T3 column (2.1 x 50 mm) (Waters, Milford MA), using a gradient elution at a flow rate of 0.4 mL/min. The mobile phase consisted of 10 mM ammonium formate in acetonitrile/water (60:40 v/v) as solvent A and 10mM ammonium formate in acetonitrile/isopropyl alcohol (10:90 v/v) as solvent B. MRM transition for all the metabolites are reported in table 2. The capillary voltage was set at 3kV. The cone voltage was set at 25V. The source temperature was set at 120°C. Desolvation gas and cone gas (N_2) flow were set to 800 and 20 l/h respectively. Desolvation temperature was set to 450°C. Detection and analysis were controlled by Waters MassLynx software version 4.1. Calibration curves were prepared for every experiment (0.1 nM to 100 nM).

Table 2: MRM transitions and MS parameters for NAPE and FAE quantification.

NAPE/FAE	Parent Ion (m/z)	Daughter Ion (m/z)	Cone Voltage	Collision Energy (V)
P18:0-22:6-N16:0	1014.8	282.3/635.5	25	20
P16:0-22:6-N18:0	1014.8	310.3/607.5	25	20
18:0-22:6-N16:0	1030.8	282.3/651.5	25	20
16:0-22:6-N18:0	1030.8	310.3/623.5	25	20
18:0-20:4-N18:0	1034.8	310.3/627.5	25	20
P18:0-22:6-N18:0	1042.8	310.3/635.5	25	20
18:0-22:6-N18:0	1058.8	310.3/651.5	25	20
18:0-22:6-N17:0	1044.6	296.4/651.5	25	20
OEA	326	62	20	30
PEA	300	62	20	30
SEA	328	62	20	30
D4-OEA	330	66	20	30
D4-PEA	304	66	20	30
D3-SEA	331	62	20	30

Activated caspase-3 ELISA

ELISA kit (R&D, Abingdon, UK) was used to measure activated Caspase-3 levels in SH-SY5Y cells. The assay was performed according to the manufacturer's instructions. Briefly, cells were grown in 6 multi-well plates, 1 h before the 6-OHDA time-point cells were treated with biotin-ZVKD-fmk inhibitor (1.4 µL), then cells were scraped with extraction buffer and stored at 4°C. 100 µL of each sample were loaded on the ELISA plate and incubated for 2 h at room temperature. Then active Caspase-3 conjugate was added to the plate and incubate for 1 h, after that substrate solution was added to each well and incubated for 30 min. Finally stop solution was added and the optical density of each well was determined using a micro-plate reader (Tecan, Mannedorf, Switzerland) set to 450 nm.

Intracellular ROS measurement

Relative changes in intracellular ROS in the SH-SY5Y cells were monitored using a fluorescent probe DCFH-DA (Abcam). Cells were grown in 24 multi-well plates and before the treatment with 6-OHDA, cells were incubated with 5 µM DCFDA for 1 h at 37°C. At the end of the treatment with 6-OHDA cells were harvested, transferred to a black multi-well plates and fluorescence was measured using a Tecan microplate reader with excitation-emission set to 485-535 nm.

Immunohistochemistry

Mice were anesthetized with chloral hydrate (400 mg/kg), and transcardially perfused with 40 mL of saline solution followed by 40 mL of 4% paraformaldehyde. Tissue was postfixed in paraformaldehyde 4% for 1 h and then stored in 30% sucrose for 3 days before being frozen in liquid nitrogen. Forty micrometer sections, one every third, were collected and processed for immunohistochemistry. In order to verify the degeneration of dopaminergic neurons, tissue immunostaining was performed by section incubation with an anti-tyrosine hydroxylase antibody (TH; 1:500; Abcam, UK) followed by incubation with Alexa fluor 546 (1:1000; Life Technologies, USA). Images were collected using a Nikon A1 confocal microscopy with a 10X magnification and a 1.4 numerical aperture objective lens. Intensity of fluorescence measurements were performed with ImageJ. The corrected total cell fluorescent was calculated according to the following formula: Integrated Density – (Area of selected cell x Mean fluorescence of background readings).

Stereology

Quantitative estimation of TH-positive neurons was performed in every 6^{th} section of the SNpc. The unbiased sampling and blinded stereological counting were done using the optical fractionator probe in Stereo Investigator software (MBF Bioscience, USA). The parameters used include a counting frame size of 60 x 60, a sampling site of 100 x 100 and a dissector height of 15 µm. A total of 3 to 4 animals per group were used and 4 sections per animal were counted.

Turning behaviour

Three weeks post-surgery all subgroups of mice received an injection of apomorphine (0.5 mg/kg in 0.2% ascorbic acid, i.p., Sigma, Milan, Italy) to evaluate the extent of nigrostriatal lesion. Rotational behavior was measured by placing animals in a circular cage where their behavior was recorded for 1 h and 15 min,

using a tracking software (Anymaze, Dublin, Ireland). The total number of rotations during the test was used for analysis.

Statistics

GraphPad Prism software V5.03 (GraphPad Software, Inc., USA) was used for statistical analysis. Data were analyzed using the Student t-test, One-way ANOVA or Two-way ANOVA followed by Bonferroni or Dunnet post hoc test for multiple comparisons. Differences between groups were considered statistically significant at values of $p < 0.05$. Results are expressed as mean ± S.E.M.

RESULTS

6-OHDA lowers NAPE-PLD expression and increases NAPE levels in SH-SY5Y cells

We first evaluated 6-OHDA toxicity on the human neuroblastoma SH-SY5Y cell line. These cells can be used in their undifferentiated form or they can be differentiated in a more pronounced neuronal phenotype. Both cases present advantages and limitations as discussed in the introduction[97]. We decided to use undifferentiated SH-SY5Y cells for two reasons: first, the differentiation process introduces a great variability between different experiments; second, undifferentiated SH-SY5Y cells already express dopaminergic markers such as tyrosine hydroxylase (TH), dopamine β hydroxilase and dopamine transporter (DAT), necessary for dopamine (DA) incorporation, in a uniform fashion.

Thus, we treated SH-SY5Y cells with 100 μM 6-OHDA and we measured the effects of the neurotoxin at different time-points. The first measure of 6-OHDA toxicity was the increase in ROS production. As shown in Fig. 7 A, ROS increase was already significant 2 h after 6-OHDA administration. This data was accompanied by a slower increase of Caspase 3 activation starting 6 h post drug administration (Fig. 7 B). Previous work has shown that NAPEs are increased after noxious stimuli (see introduction), thus I analyzed levels of these lipid mediators. As expected, 6-OHDA toxicity was accompanied by an increase in diverse species of NAPE, mainly species with a long polyunsaturated chain in the *sn2* position (Fig. 7 C), which are PEA and SEA precursors. NAPE increase was accompanied by a progressive reduction in both mRNA and protein expression of NAPE-PLD, the enzyme that catalyses NAPE hydrolysis (Fig. 7 D-E).

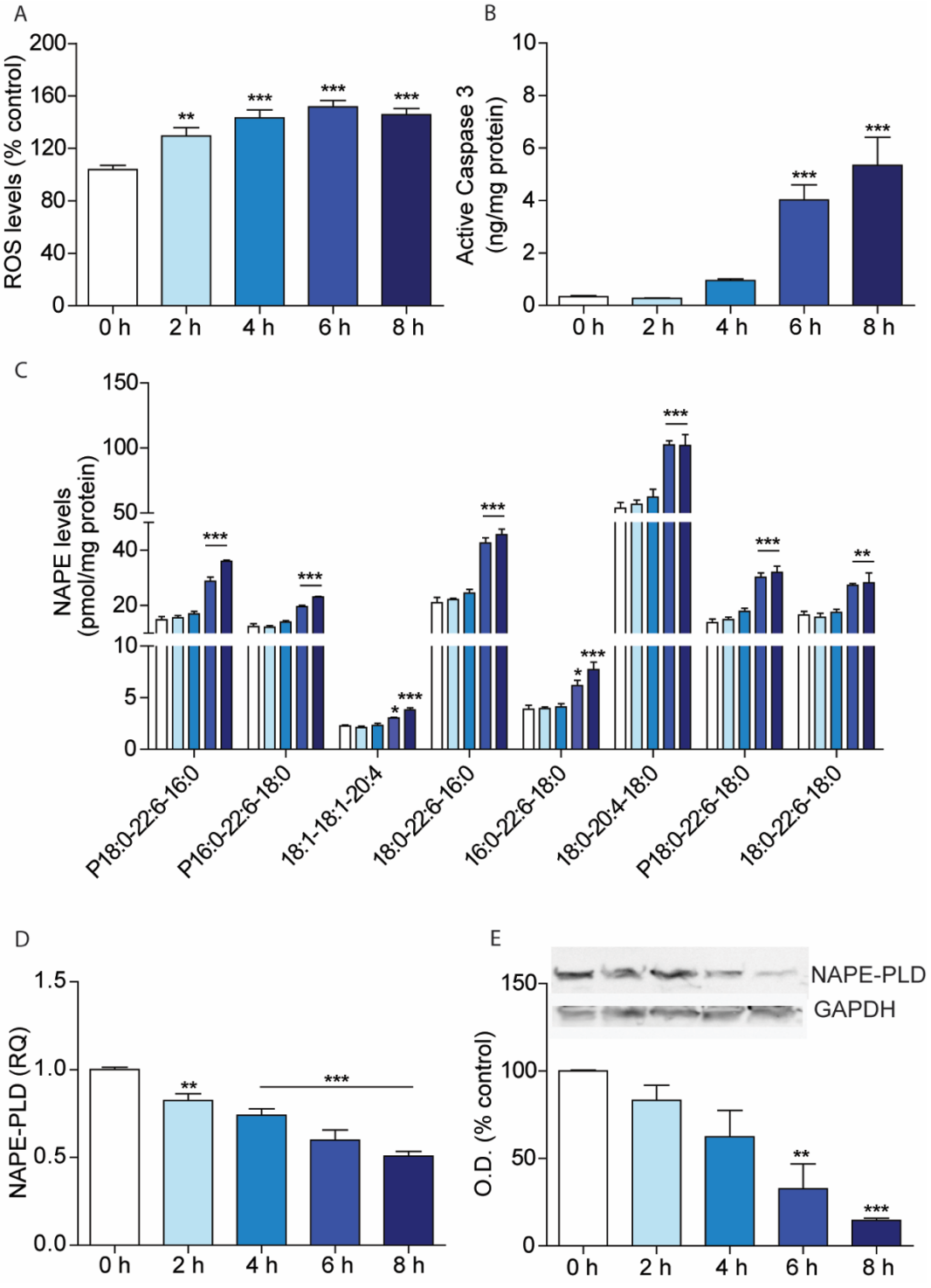

Figure 7: Time-course of the effect of 100 µM 6-OHDA on SH-SY5Y cells. *(A) ROS, (B) Active Caspase-3, (C) NAPEs levels; (D) NAPE-PLD mRNA expression levels; (E) NAPE-PLD protein expression. All histograms represent the mean +/- SEM of 6-9 determinations from three independent experiments. *p<0.05, **p<0.01, ***p<0.001. One-Way ANOVA followed by Bonferroni's test.*

NAPE-PLD silencing protects SH-SY5Y cells from 6-OHDA toxicity

To address whether NAPEs have a protective or noxious effect on neuronal viability, I used a small interference RNA technique to induce NAPE-PLD mRNA down-regulation , which was effectively reduced by 61% (Fig. 8 A). SHSY5Y cells are not widely used for this technique, as neurons are not so prone for transfection, thus we consider a downregulation of 60% a good result, comparable to the 70% efficiency suggested by the manufacturer's protocol.

6-OHDA induced a higher increase in NAPE levels in NAPE-PLD silenced cells when compared to control cells (Fig. 8 B) without affecting FAE levels (Fig. 8 C). At a functional level, NAPE-PLD silenced cells produced less ROS (Fig. 8 D), and a weaker activation of Caspase 3 (Fig. 8 E) than did control cells. As a consequence, cell death was reduced in silenced cells compared to naïve cells (Fig. 8 F); thus, NAPE species can reduce 6-OHDA-induced toxicity in SH-SY5Y cells. We then confirmed the protective role of NAPEs, using a pharmacological approach: we treated SH-SY5Y cells with ARN19874, a NAPE-PLD inhibitor developed in our laboratory. Cells were pre-treated with ARN19874 (50 μM) 2 h before 6-OHDA administration and then counted after 8 h of 6-OHDA treatment. As expected, NAPE-PLD inhibition produces an effect similar to that of NAPE-PLD silencing, leading to an increase in the number of viable cells (Fig. 8 G). In contrast when NAPE-PLD is overexpressed (Fig. 8 A), SH-SY5Y cells were more sensitive to 6-OHDA toxicity (Fig. 8 H), confirming the protective role of NAPEs.

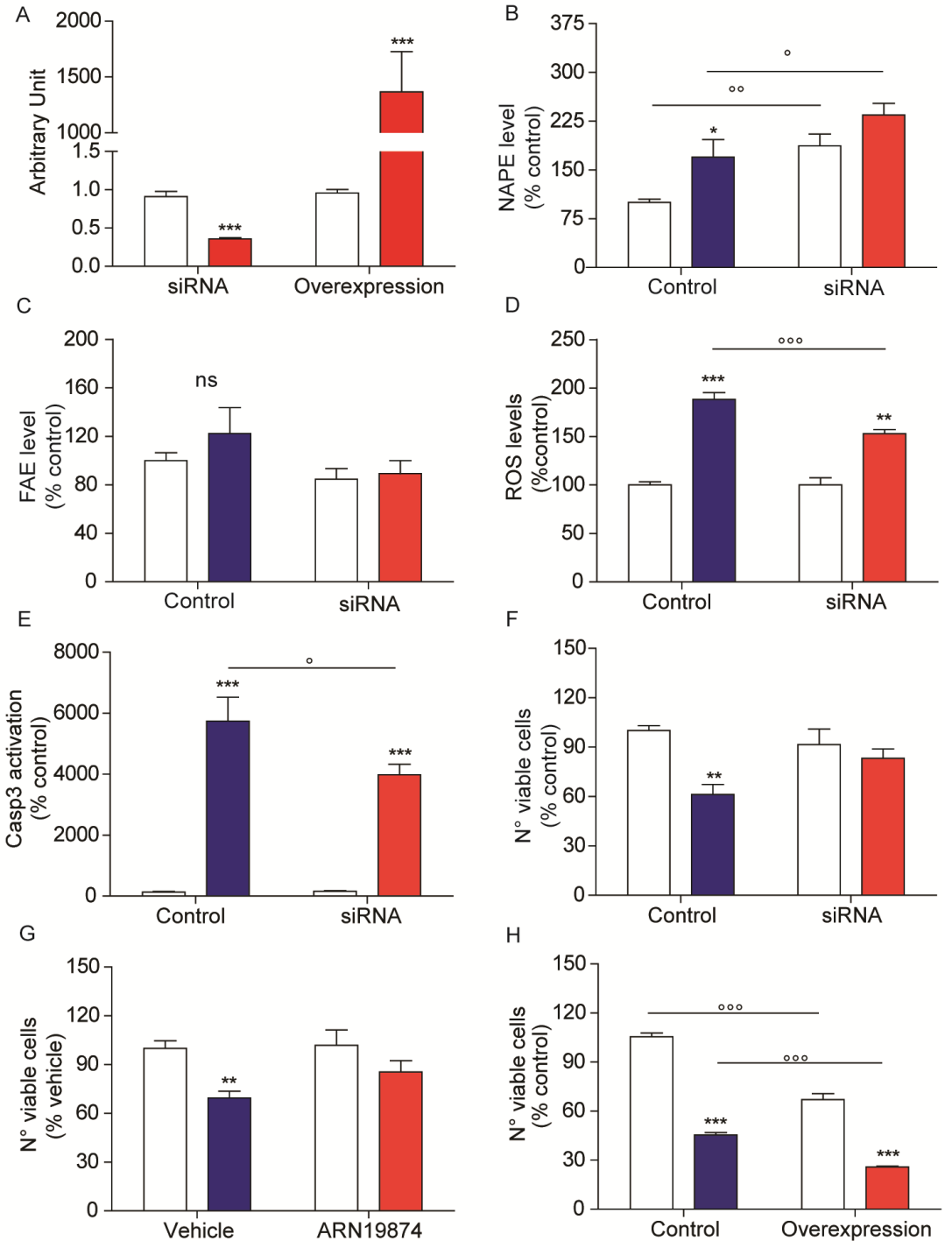

Figure 8: Effect of NAPE-PLD silencing in 100 µM 6-OHDA treated SH-SY5Y cells*. (A) NAPE-PLD mRNA expression after silencing and overepression; (B) NAPE and (C) FAE levels measured 8h after the treatment; (D) ROS and (E) Active Caspase-3 levels respectively 8 and 6 h after treatment; cell viability in NAPE-PLD silenced cells (F), in cells pre-treated with ARN19874 (G), and in NAPE-PLD overexpressing cells (H). All histograms represent the mean +/- SEM of 6-9 determinations from three independent experiments. In white vehicle, in blue 6-OHDA treated naïve cells, in red 6-OHDA treated silenced/inhbited/overexpressed cells. *p<0.05, **, p<0.01, ***p<0.001 comparing 6-OHDA to control, °p<0,05, °°p<0,01, °°°p<0,001 comparing siRNA to Control. Two-Way ANOVA followed by Bonferroni's test.*

NAPE-PLD deletion protects from 6-OHDA toxicity in a mouse model of Parkinson's disease

We next moved to an in vivo approach, using NAPE-PLD$^{-/-}$ mice. We have already shown that specific NAPE species are increased after unilateral administration of 6-OHDA in the CPu of mice[13]: these lipid molecules show saturated or mono-unsaturated acyl chains in the *sn1* position, long polyunsaturated chains in the *sn2* position, and are mainly PEA and SEA precursors. Thus, using the same model, we investigated the role of these molecules using NAPE-PLD$^{-/-}$ mice[28].

Briefly, we injected 3.2 mg/ml of 6-OHDA in two areas of the Caudate of mice. We then collected CPu and SNpc from lesioned or control side of the brain 48 h or 3 weeks after lesion. 48 h after drug administration, NAPE-PLD$^{-/-}$ mice showed a basal increase in NAPE levels (Fig. 9 A-B) and, as expected, treatment with 6-OHDA induced an additional increase in these lipids in the CPu (Fig. 9 B). Three weeks after 6-OHDA injection, when the pathology is fully developed, we conducted histological studies on the brains of NAPE-PLD$^{-/-}$ mice and wild type littermates. CPu and SNpc were stained with anti-Tyrosine Hydroxylase (TH) antibody. TH is expressed specifically in dopaminergic neurons, thus TH staining represents a good approach to measure dopaminergic neurodegeneration. NAPE-PLD$^{-/-}$ mice showed a reduction in the degeneration of dopaminergic neurons in the substantia nigra pars compacta compared to wild type mice (Fig. 9 C-E); this effect was further quantified through the count of TH positive neurons using a stereological approach, which allows to obtain an unbiased and quantitative estimation of the number of specific objects, through the use of random and systematic sampling. This technique highlights protective effect of NAPE-PLD deletion (Fig. 9 G): wild type littermates lost 69% of dopaminergic neurons in the SNpc, whereas NAPE-PLD$^{-/-}$ mice lost only 20% of TH positive neurons. Moreover, unilateral lesion induces an imbalance in the dopaminergic system between control and lesion side of the brain, which can be quantified by administration of apomorphine, a dopaminergic agonist. This compound induced vigorous ipsilateral rotations, because of hypersensitivity of the dopaminergic receptors in the lesioned emisphere. The number of rotations is directly proportional to the magnitude of the lesions. Thus, using this technique we observed a 51% reduction in the number of rotations induced by apomorphine in NAPE-PLD$^{-/-}$ mice compared to wild-type mice (Fig. 9 H).

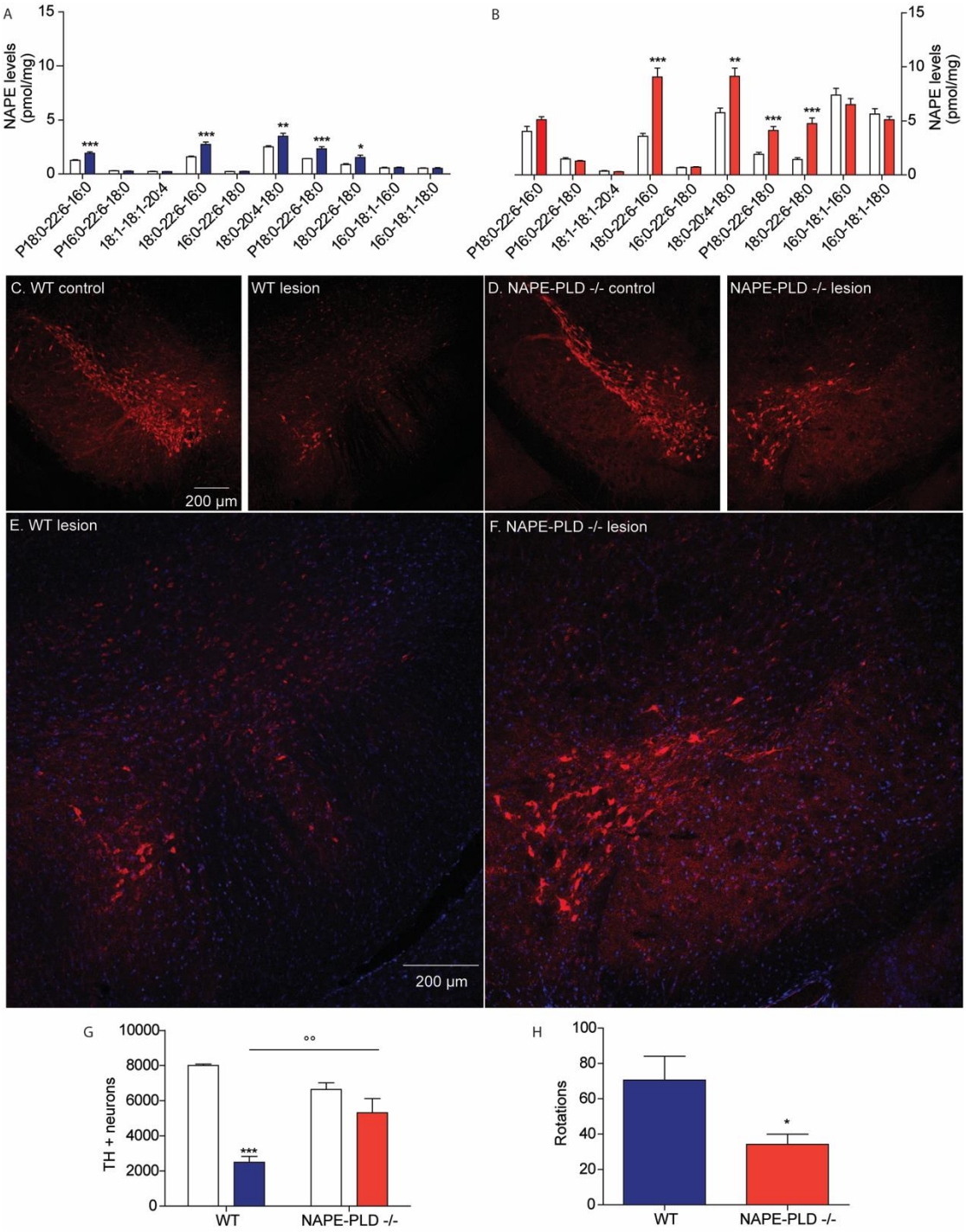

Figure 9: Protective effect of NAPE-PLD depletion in 6-OHDA mice model. *(A-B) NAPEs levels in wild type mice treated with 6-OHDA (A) compared to NAPE-PLD$^{-/-}$ mice (B). (C-F) Staining for TH (Red) and DAPI (Blue) in contralateral side brain (Control) or ipsilateral side brain (Lesion) of WT mice (C, E), compared to contralateral side brain or ipsilateral side brain of NAPE-PLD KO mice (D, F). (G) Count of TH+ neurons, (H) Number of apomorphine induced rotation in NAPE-PLD$^{-/-}$ mice compared to WT mice. All histograms represent the mean +/- SEM of 3-9 determinations from three independent experiments. *p<0.05, **p<0.01, ***p<0.001; °°p<0.01 comparing WT versus KO. Student's t test or Two-Way ANOVA followed by Bonferroni's test.*

In the CPu, 3 weeks post surgery, we observed an increased number of dopaminergic fibers in NAPE-PLD$^{-/-}$ mice (Fig. 10 A-D); indeed, the quantification of fluorescence intensity (Fig. 10 E) showed that wild type mice lost 61% of the dopaminergic fibers in the CPu, while NAPE-PLD$^{-/-}$ mice only 26%. Taken together, these data suggest that NAPE species have a protective role during the neurodegenerative process.

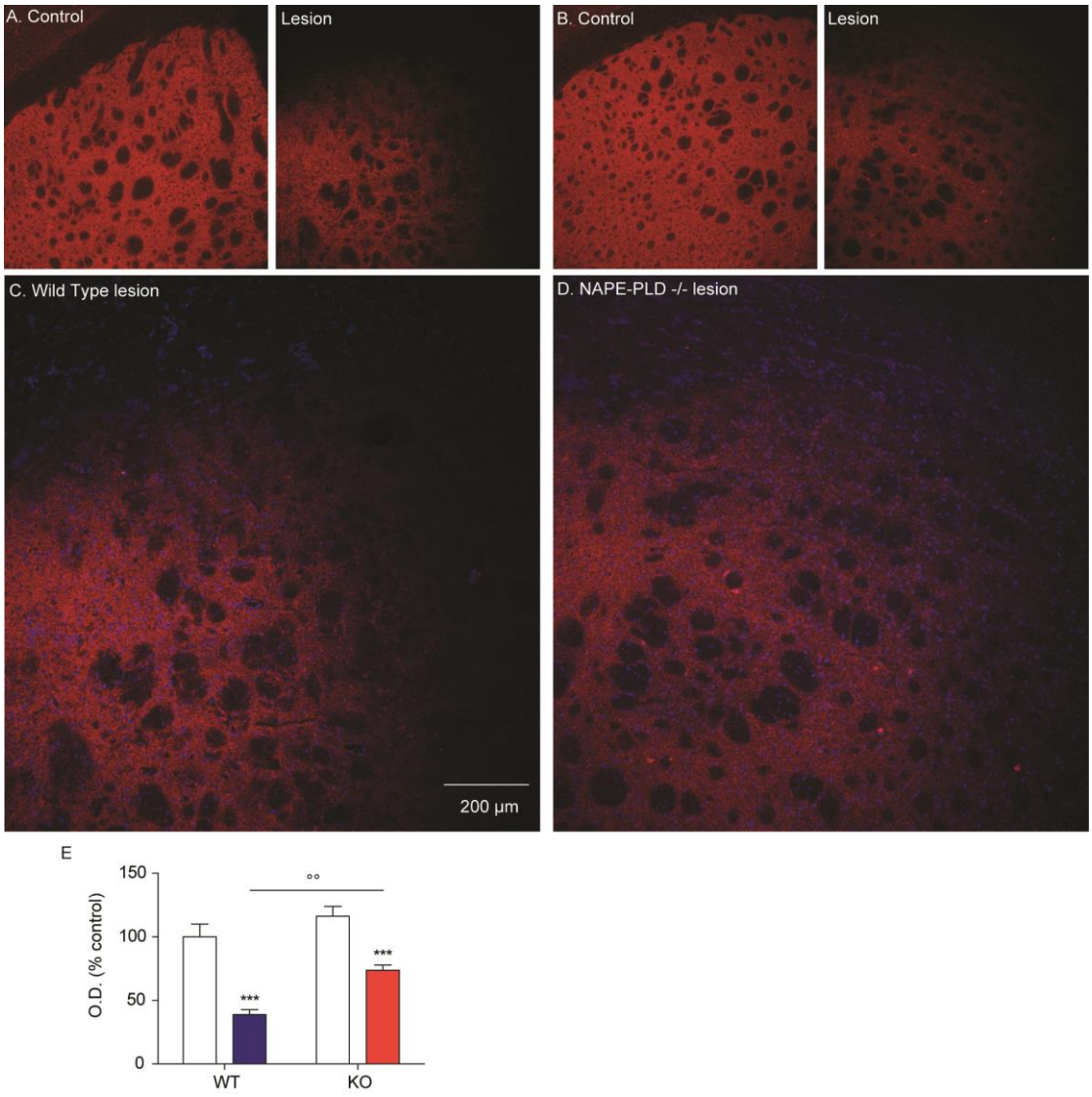

Figure 10: Protective effect of NAPE-PLD depletion in 6-OHDA mice model. *(A-D) Staining for TH (Red) and DAPI (Blue) in contralateral side brain (Control) or ipsilateral side brain (Lesion) of WT mice (A,C), compared to contralateral side brain or ipsilateral side brain of NAPE-PLD KO mice (B,D). (E) intensity of fluorescence of TH staining in the Caudate Putamen of NAPE-PLD$^{-/-}$ control and lesion side brain, compared to wild type mice. All histograms represent the mean +/- SEM of 19-26 determinations from three independent experiments. *p<0.05, **p<0.01, ***p<0.001; °p<0.05, °°p<0.01, °°°p<0,001 comparing WT versus KO. Two-Way ANOVA followed by Bonferroni's test.*

NAPE-PLD deletion is linked to peculiar genic modifications that may be involved in neuroprotection

To explore the mechanisms underlying neuroprotection in NAPE-PLD$^{-/-}$ mice, I used a RT² Profiler™ PCR Array approach. Briefly, mRNA obtained from control and lesioned side SNpc, collected 48 h post 6-OHDA administration, was amplified on a commercial mRNA array plate containing primers for genes directly or potentially involved in PD etiology. This technique led me to assess mRNA expression changes between WT and KO mice in response to 6-OHDA-induced toxicity.

The analysis was designed to reveal separately possible differential effects of 6-OHDA on the two strains (Fig. 11 A, B respectively). Statistical analysis revealed multiple but significant differences in PD-related gene expression between the lesioned side and control side of the two groups. Among 84 assayed genes, 25 were shown to be regulated in an opposite direction in the two strains, as reported in Table 3. In particular, only 15 genes (Fig. 11 C,D) showed a difference of at least 25% in expression between lesioned sides of the two strains. Considering functional gene groups assayed, the most abundant gene expression changes were observed for genes related to cell adhesion (Apc, App, Cdh8, Nfasc, Fn1), cytoskeletal organization (Apc, PARK2, Mapt), ubiquitination (LRRK2, PARK2, PINK1), mitochondria (LRRK2, PINK1, Casp7) and membrane transport (Syt11, Egln1, Slc18a2). However, most of the genes are known to be involved in more than one process. It is worth of note that three genes related to genetic and sporadic PD (LRRK2, PARK2 and PINK1) were regulated in an opposite way in the two strains. In particular, PARK2 and PINK1, which are characterized by a loss of function in the pathology of PD, were down-regulated in WT mice (-48% and -20% respectively), while slightly up-regulated in KO mice (+9%); moreover, two substrates of PARK2-mediated ubiquitination (Atxn3, Syt11) were downregulated in WT mice after the lesion (-25% and -29%), and slight up-regulated in KO mice (+10% and +7%). Lastly, LRRK2 is known to be mutated in a gain of function fashion in many PD cases: in accordance, WT mice up-regulated this gene in response to 6-OHDA administration (+15%); in contrast, KO mice markedly down-regulated the gene by 50%.

Table 3: PD related genes expression fold change in NAPE- PLD$^{-/-}$ and WT mice 48h after 6-OHDA administration. *FR fold regulation. P value calculated by Student's t test, with n=3.*

Gene symbol	FR WT	% WT	p value	FR KO	% KO	p value
Apc	-1.45	-45%	0.046506	1.12	+12%	0.647152
App	-1.23	-23%	0.014865	1.06	+6%	0.828518
Atp2b2	-1.03	-3%	0.765594	1.09	+9%	0.841150
Atxn3	-1.25	-25%	0.030927	1.10	+10%	0.706594
Casp1	-1.05	-5%	0.702875	1.11	+11%	0.860526
Casp 7	-1.30	-30%	0.379677	1.05	+5%	0.893019
Casp9	-1.42	-42%	0.006829	1.06	+6%	0.932468
Cdh8	1.07	+7%	0.613042	-1.52	-52%	0.294888
Egln1	-1.21	-21%	0.036793	1.03	+3%	0.954444
Fbxo9	-1.14	-14%	0.141198	1.00	0%	0.975173
Fn1	-1.34	-34%	0.108515	1.23	+23%	0.656451
Gbe1	-1.07	-7%	0.550695	1.09	+9%	0.269209
Hspa4	-1.20	-20%	0.068983	1.05	5%	0.601453
LRRK2	1.15	+15%	0.351875	-1.50	-50%	0.102601
Mapt	-1.22	-22%	0.012189	1.05	+5%	0.631354
Nfasc	-1.14	-14%	0.103517	1.31	+31%	0.174574
Park2	-1.48	-48%	0.092555	1.09	+9%	0.797287
PINK1	-1.20	-20%	0.100158	1.09	+9%	0.774096
Prdx2	-1.08	-8%	0.281470	1.01	+1%	0.947735
Slc18a2	1.71	+71%	0.742609	-1.16	-16%	0.584880
Slc25a4	-1.08	-8%	0.431641	1.03	+3%	0.760694
Syt11	-1.29	-29%	0.007682	1.07	+7%	0.893016
Uba1	-1.15	15%	0.339637	1.03	+3%	0.582091
Ubc	-1.14	14%	0.215492	1.07	+7%	0.619278
Vamp1	1.00	0%	0.929908	-1.15	-15%	0.612199

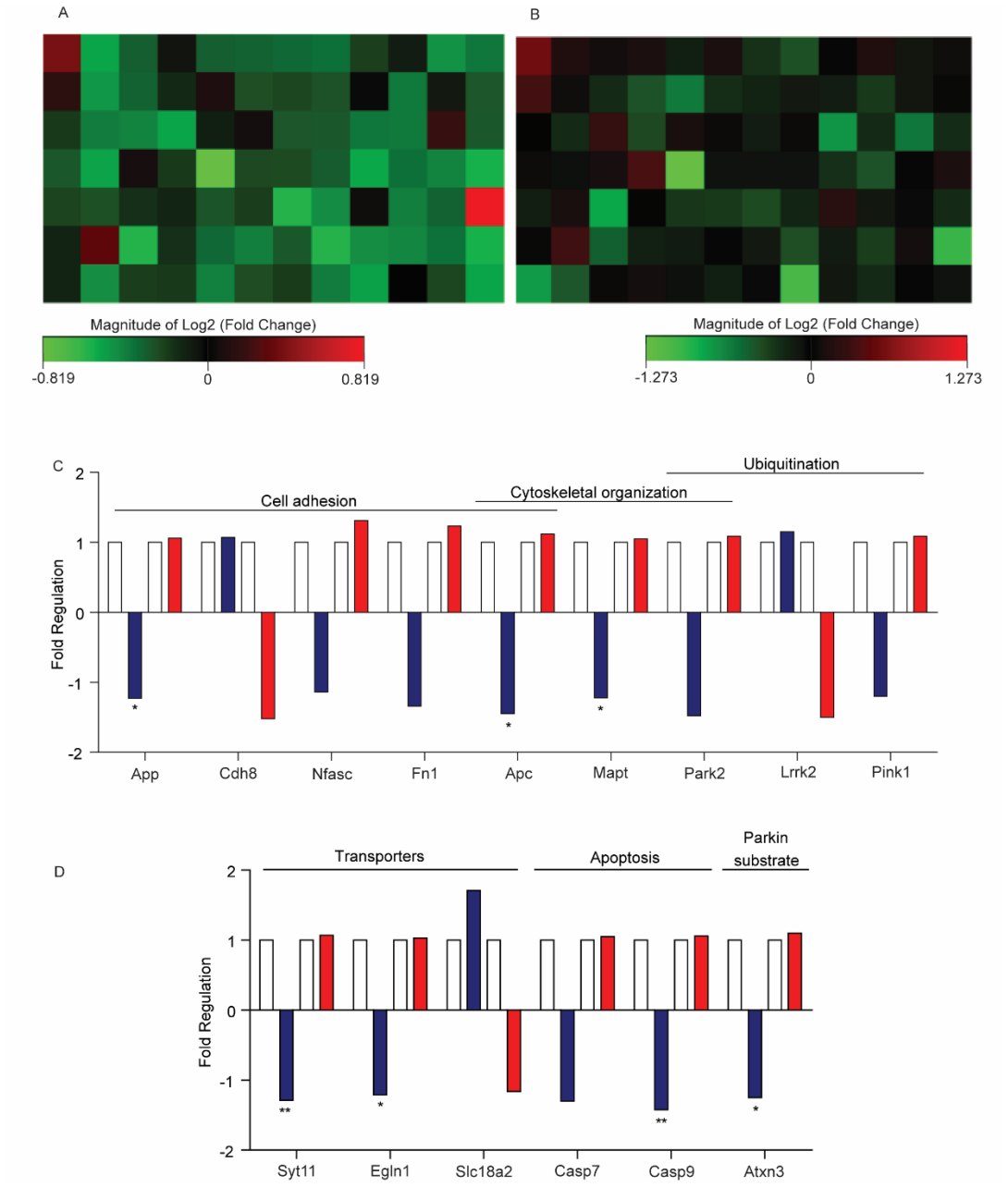

Figure 11: Different gene regulation in NAPE- PLD$^{-/-}$ and WT mice 48h after 6-OHDA administration. *Heatmap of gene regulation in WT mice (A) and NAPE- PLD$^{-/-}$ mice (B) after 6-OHDA administration compared to control side brains. (C,D) Fold regulation change expression of genes involved in cell adhesion, cytoskeletal organization and ubiquitination (C) or in transport, apoptosis and parkin substrate (D). *p<0.05, **p<0.01, comparing lesioned side versus control side brain. Student's t-test.*

NAPE-PLD$^{-/-}$ mice show a downregulation of LRRK2 pathway

To further verify PARK2, PINK1 and LRRK2 expression in NAPE-PLD$^{-/-}$ and wild type mice, I run an RT-PCR analysis on samples collected 48 h post lesion. The results did not reveal any statistically significant change in LRRK2 transcriptions between lesioned and unlesioned side of WT mice (Fig. 12 A), while showing a significant upregulation of PARK2 in NAPE-PLD$^{-/-}$ lesioned mice and only a positive trend in the control side (Fig. 12 B). No effect of the lesion on NAPE-PLD deletion was seen in the levels of PINK1transcription (Fig. 12 C).

Given the strict association of LRRK2 with membranes, I finally focused my attention on this protein. LRRK2 is a large ubiquitous cytoplasmic protein with multiple functional domains, encompassing two enzymatic functions at its core: GTPase and kinase activities. It participates in a range of cellular processes such as vesicular trafficking, cytoskeletal dynamics, mitochondrial function and autophagy[98]. As already mentioned, LRRK2 mutations are common in sporadic and familiar PD, in particular, the dominant pathogenic mutations described up to date occur within the enzymatic core of this protein, leading to a gain of function.

This protein mediates its function regulating diverse signaling cascades. Indeed, LRRK2 is known to bind multiple small GTPases such as Rho GTPase proteins. Among other proteins it binds Rac1, regulating positively the site of action of this small GTPase[99].

Rac1 (Ras-related C3 botulinum toxine substrate 1) is a signaling GTPase, belonging to the Ras superfamily. This protein is known to be involved in many cellular processes, including cell growth, cytoskeletal reorganization cell adhesion and motility. Furthermore it is known to be involved in the regulation of cell fate in neurodegeneration[100].

Western blot analyses on lesioned and control SNpc isolated 48 h post 6-OHDA administration were performed in both WT and KO mice. Interestingly, LRRK2 protein expression was strongly downregulated in the control side of KO mice compared to WT mice, with a decrease of about 52% (Fig. 12 D). LRRK2 downregulation was accompanied by an increase in total Rac1 expression in KO mice (Fig. 12 E), but not in activated Rac1 (Rac1-GTP in Fig. 12 F). Indeed, Fig. 12 G shows the rate between total Rac1 and Rac1-GTP, confirming the inhibition of Rac1 activity in KO mice. Moreover, Focal adhesion kinase (FAK-1), another protein known to stimulate Rac1 activity, was also down-regulated in NAPE-PLD$^{-/-}$ mice (Fig. 12 H).

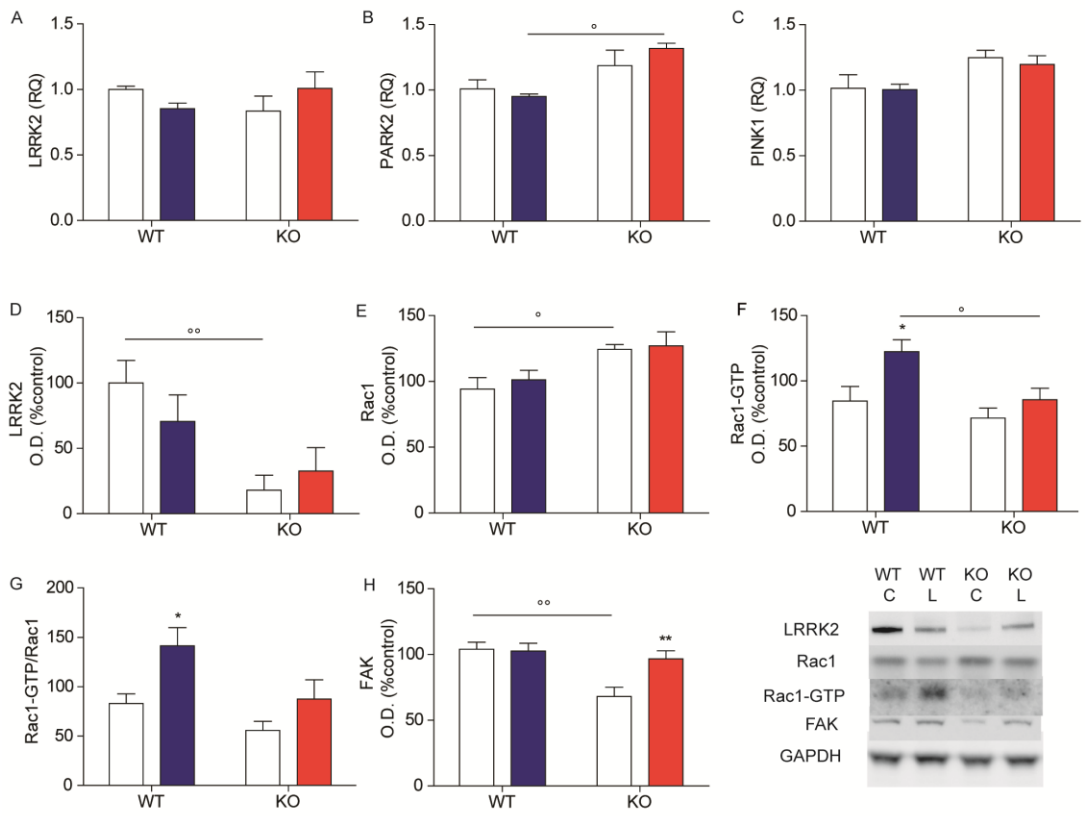

Figure 12: NAPE-PLD depletion leads to a downregulation of LRRK2 pathway. *LRRK2 (A), PARK2 (B), PINK1 (C) mRNA expression levels in the control (white) or lesioned side of substantia nigra in NAPE-PLD$^{-/-}$ and WT mice (respectively red and blue). LRRK2 (D), Rac1 (E), Rac1-GTP (F) and FAK1 (H) protein levels, measured by western blot in control and lesioned side brain of NAPE-PLD$^{-/-}$ and WT mice. (G) Rate of Rac1-GTP on total Rac1. All histograms represent the mean +/- SEM of 6 determinations from three independent experiments. *p<0.05, **p<0.01; °p<0.05, °°p<0,01 comparing WT versus KO Two-Way ANOVA followed by Bonferroni's test.*

DISCUSSION

NAPEs have been primarily conceptualized as precursors for bioactive FAEs, such as anandamide and PEA. Only in the last decade, the scientific community has started to think about NAPEs as lipid mediators with specific functions, separate from those of FAEs, such as membrane stabilization, anchorage or activation of peripheral membrane proteins and organization of cell division sites[5].

NAPEs accumulate in the brain after injury.

In the present work, I investigated the role of these membrane compounds in the neurodegenerative process that underlies PD progression. To do so, I first focused my attention on a cellular model of PD, in which I confirmed increased NAPEs production after 6-OHDA administration. Moreover, impairment of the respiratory mechanism leads to an increase of intracellular calcium, which could stimulate the activity of Ca-NAT, the enzyme that produces NAPEs.

Unfortunately, Ca-NAT has not yet been isolated and characterized, so we can only manage indirectly NAPEs accumulation, through the inhibition of the downstream metabolism of NAPEs. Thus, using a genetic approach, I demonstrated that NAPEs have a protective role in SH-SY5Y cells. Indeed, silencing of NAPE-PLD, the main enzyme involved in NAPE degradation, induced a further increase in NAPEs but not in FAE levels, protecting cells from 6-OHDA induced toxicity.

Here, I demonstrated for the first time that NAPEs are produced in a cellular model of PD; moreover, we have recently observed that particular species of NAPEs are produced also *in vivo*, in a mice model of PD, following administration of 6-OHDA in the CPu[13].

From this starting point, I next demonstrated that NAPE-PLD$^{-/-}$ mice show a reduction in the neurodegenerative process, compared to WT mice. Indeed, the stereological count of TH positive neurons and dopaminergic fibers, together with behavioral tests confirm the protective role of NAPEs. In particular, NAPE-PLD$^{-/-}$ mice showed a baseline increase in all NAPE species analyzed, but 6-OHDA treatment induced a further increase in specific NAPE compounds; namely PEA and SEA precursors (with 16:0 or 18:0 chain in the *sn3* position, respectively) and long polyunsaturated carbons chains (mainly 22:6) in the *sn2* position.

The baseline increase in NAPE levels is accompanied by a substantial difference in gene expression between NAPE-PLD$^{-/-}$ mice and their WT littermates. This is the

reason why analyzing data from mRNA array panel, I decided to consider separately the two strains of mice, comparing gene expression in lesioned brain side versus control side brain.

Among the 15 genes that were regulated in an opposite fashion in the two strain, some of them are poorly characterized in PD: Cadherin 8 is only known to be overexpressed in LUHMES cells treated with 6OHDA[101]; Fibronectin 1 is reported to represents a protective factor in PD. In both cases our data fit with these evidences, indeed Cdh8 is downregulated in WT mice and upregulated in KO mice, while Fn 1 showed an opposite behavior.

Other genes are better characterized in relation to PD, but the literature reports controversial data; for instance, Ataxin 3 is reported to be upregulated in human SNpc from PD patients[102] and in PC12 cells treated with 6OHDA[103], while is downregulated in LUHMES cells treated with 6-OHDA[101] as in our model. Caspase 9 is known to be overexpressed in MPTP- or rotenone-treated mice[104,105], but is downregulated in SH-SY5Y cells treated with paraquat[106]. My data are in accordance with the latter paper: WT mice showed downregulation of Caspase 9, while KO mice slight up-regulated it.

Caspase 7, Egln1 and Slc18a2 are differentially regulated in NAPE-PLD$^{-/-}$ mice, comparing to previous data; indeed Caspase 7 and Egln1 are upregulated in a variety of models[101, 103, 106,107] , while Slc18a2 is known to be downregulated[101,108].

Moreover, data obtained from mRNA arrays highlighted a peculiar difference between NAPE-PLD$^{-/-}$ mice and WT in 3 genes that are strongly linked with PD: PARK2, PINK1 and LRRK2[48]. PARK2 encodes for parkin, an ubiquitin ligase protein, while PINK1 correspond to the PTEN induced putative kinase 1; these proteins are involved in a quality control pathway that maintains mitochondrial homeostasis in many cell types, including dopaminergic neurons, whose malfunction causes PD[109]. Indeed, both these proteins are mutated in many cases of early-onset familial PD. Generally, mutations determine a loss of function in these proteins, leading to an impairment of the ubiquitin-proteasome pathway[110]. Thus, overexpression of PARK2 and PINK1 have a protective effect on 6-OHDA induced toxicity[111,112]. In our model PARK2 and PINK1 are downregulated in WT mice treated with 6-OHDA, while slightly up-regulated in NAPE-PLD$^{-/-}$ mice. PARK2 upregulation in the lesioned side of NAPE-PLD$^{-/-}$ mice was further confirmed by RT-PCR. Consistent with our observations, these two proteins were down-regulated in LUHMES cells treated with 6-OHDA[101]. Moreover, PINK1 is known to be

downregulated in the SNpc of subjects with PD[113]. We may speculate that parkin and PINK1 up-regulation in NAPE-PLD$^{-/-}$ mice participate in the neuroprotective effects of NAPEs.

Interestingly, a combined analysis obtained using two different softwares that illustrate known protein-protein interactions, available online (https://thebiogrid.org and http://string-db.org), showed that some of the proteins coded by the genes highlighted by the arrays are linked together (Fig. 13). I chose to focus my attention on a smaller set of proteins because our data are in agreement with the literature, and these genes are already well characterized in PD. Probably, the beneficial effect induced by NAPEs is the readout of a complex interaction between all these proteins, rather than the result of a single protein modulation.

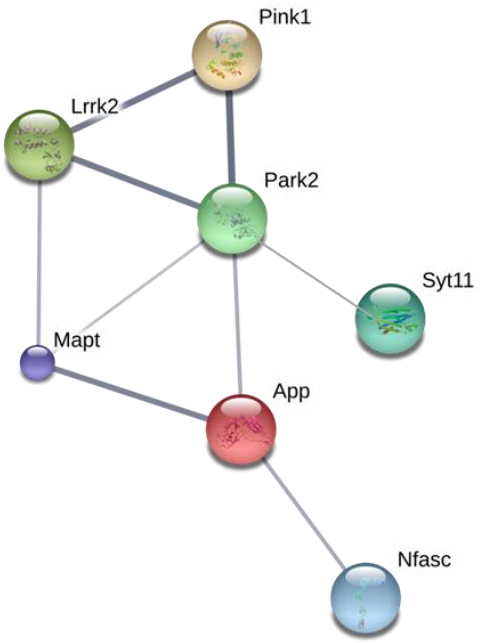

Figure 13: Protein-protein interaction analysis. *Protein regulated in an opposite fashion in NAPE-PLD$^{-/-}$ and WT mice that are linked by interactive capability. The software I adopted, run their analysis using databases that analyze the whole literature. The more is thick the line between two proteins, the more their interaction is consistent.*

The LRRK2 gene encodes for LRRK2 protein also known as Dardarin, a large multifunctional protein containing diverse domains; including a kinase domain and a GTPasic core. LRRK2 is known to have many functions in the cells, mainly related to cellular trafficking and regulation of actin dynamics[114]. LRRK2 is mutated in a consistent number of PD patients, with the most common abnormalities determining a gain of function of the protein, and affecting either the kinase domain or the GTPase portion[115].

Our arrays studies highlighted differential regulation of LRRK2: it is slightly upregulated in the lesioned side of WT mice, whereas it is downregulated in NAPE-PLD$^{-/-}$ lesioned side. However, when we quantified protein expression, surprisingly the protein appeared to be strongly downregulated in unlesioned KO mice compared to WT. Given the fact that LRRK2 is frequently associated with cellular membranes, we speculate that enrichment of membranes in NAPE content leads to a minor binding capability of LRRK2, which accumulates in the cytosol and is degraded. We are currently testing this hypothesis.

LRRK2 is known to bind and activate Rac1[99], a small GTPase that has been shown to be inhibited by NAPE[32]. In NAPE-PLD$^{-/-}$ mice, it seems that lack of LRRK2 determines an inhibition in Rac1 activity, but not a reduction in the total form of Rac1 protein, which appears to be upregulated, maybe as a compensation effect.

Rac1 is involved in a variety of functions such as cell growth, cytoskeletal reorganization, cell adhesion and motility. In neurodegeneration, the role of Rac1 activity is controversial: it is reported that its activation leads to the activation of the ERK/MAPK and PI3K/AKT pathways, which both determine activation of pro-survival Bcl-2 family and inhibition of pro-apoptotic Bcl2 family. At the same time, it is also known that Rac1 activation leads to the stabilization of the NADPH oxidase on cell membranes, determining ROS production[100].

On the basis of my results, Rac1 could be involved in NADPH oxidase stabilization in the SNpc, thus if inhibited leads to the reduction of ROS production, as we have already observed in NAPE-PLD silenced SH-SY5Y cells.

Consistent with this hypothesis, it is known that Rac1 mediates noxious effect in neurodegeneration both *in vitro* as *in vivo*[116]: SH-SY5Y cells treated with glutamate[117] or in the presence of proinflammatory cytokines[118] showed translocation of Rac1 to the plasma membrane, subsequent stabilization of NADPH oxidase, cytoskeleton reorganization and ROS induced cell death. The same pathway has been observed also in ischemic mice[119,120], where the inhibition of Rac1 appears to be protective from neurodegeneration.

In our models, Rac1 inhibition could be mediated by both LRRK2 and FAK1, given the fact that both this proteins impact Rac1 activation[99,121] and are inhibited or downregulated in NAPE-PLD$^{-/-}$mice.

In conclusion, our multidisciplinary experiments provide strong evidence that NAPEs play a protective role in the response to 6-OHDA induced toxicity. Indeed, NAPEs induce changes in gene expression that could cooperate in mediating

neuroprotective effects. In particular, NAPEs lead to LRRK2 downregulation and consequent Rac1 inhibition, possibly determining a reduction in ROS production.

This work could represent the starting point for the development of new therapeutic approaches and identification of new biological markers for neurodegenerative diseases, in particular for Parkinson’s Disease.

REFERENCES

1. Cadas, H., Schinelli, S. & Piomelli, D. Membrane localization of N-acylphosphatidylethanolamine in central neurons: Studies with exogenous phospholipases. in *Journal of Lipid Mediators and Cell Signalling* **14,** 63–70 (1996).
2. Lo Verme, J. *et al.* The nuclear receptor peroxisome proliferator-activated receptor-alpha mediates the anti-inflammatory actions of palmitoylethanolamide. *Mol. Pharmacol.* **67,** 15–9 (2005).
3. Fride, E. & Mechoulam, R. Pharmacological activity of the cannabinoid receptor agonist, anandamide, a brain constituent. *Eur. J. Pharmacol.* **231,** 313–314 (1993).
4. Piomelli, D. A fatty gut feeling. *Trends in Endocrinology and Metabolism* **24,** 332–341 (2013).
5. Coulon, D., Faure, L., Salmon, M., Wattelet, V. & Bessoule, J. J. Occurrence, biosynthesis and functions of N-acylphosphatidylethanolamines (NAPE): Not just precursors of N-acylethanolamines (NAE). *Biochimie* **94,** 75–85 (2012).
6. Shangguan, T., Pak, C. C., Ali, S., Janoff, A. S. & Meers, P. Cation-dependent fusogenicity of an N-acyl phosphatidylethanolamine. *Biochim. Biophys. Acta - Biomembr.* **1368,** 171–183 (1998).
7. Mileykovskaya, E. *et al.* Phosphatidic acid and N-acylphosphatidylethanolamine form membrane domains in Escherichia coli mutant lacking cardiolipin and phosphatidylglycerol. *J. Biol. Chem.* **284,** 2990–3000 (2009).
8. Natarajan, V., Schmid, P. C. & Schmid, H. H. O. N-Acylethanolamine phospholipid metabolism in normal and ischemic rat brain. *Biochim. Biophys. Acta - Lipids Lipid Metab.* **878,** 32–41 (1986).
9. Hansen, H. H., Ikonomidou, C., Bittigau, P., Hansen, S. H. & Hansen, H. S. Accumulation of the anandamide precursor and other N-acylethanolamine phospholipids in infant rat models of in vivo necrotic and apoptotic neuronal death. *J. Neurochem.* **76,** 39–46 (2001).
10. Hansen, H. H., Hansen, S. H., Schousboe, A. & Hansen, H. S. Determination of the phospholipid precursor of anandamide and other N- acylethanolamine phospholipids before and after sodium azide-induced toxicity in cultured neocortical neurons. *J. Neurochem.* **75,** 861–871 (2000).
11. Hansen, H. S., Lauritzen, L., Strand, A. M., Moesgaard, B. & Frandsen, A. Glutamate stimulates the formation of N-acylphosphatidylethanolamine and N-acylethanolamine in cortical neurons in culture. *Biochim. Biophys. Acta* **1258,** 303–308 (1995).
12. Saito, M. *et al.* Involvement of ceramide in ethanol-induced apoptotic neurodegeneration in the neonatal mouse brain. *J. Neurochem.* **115,** 168–177 (2010).
13. Basit, A., Pontis, S., Piomelli, D. & Armirotti, A. Ion mobility mass spectrometry enhances low-abundance species detection in untargeted lipidomics. *Metabolomics* **12,** 50 (2016).

14. Dauer, W. & Przedborski, S. Parkinson ' s Disease : Mechanisms and Models. *Neuron* **39,** 889–909 (2003).

15. Nutt, J. & Wooten, G. F. Clinical Practice. Diagnosis and initial management of Parkinson's disease. *N. Engl. J. Med.* **353,** 1021–1027 (2005).

16. Rahman, I. A. S., Tsuboi, K., Uyama, T. & Ueda, N. New players in the fatty acyl ethanolamide metabolism. *Pharmacological Research* **86,** 1–10 (2014).

17. Wellner, N., Diep, T. A., Janfelt, C. & Hansen, H. S. N-acylation of phosphatidylethanolamine and its biological functions in mammals. *Biochimica et Biophysica Acta - Molecular and Cell Biology of Lipids* **1831,** 652–662 (2013).

18. Gillum, M. P. *et al.* N-acylphosphatidylethanolamine, a Gut- Derived Circulating Factor Induced by Fat Ingestion, Inhibits Food Intake. *Cell* **135,** 813–824 (2008).

19. Ogura, Y., Parsons, W. H., Kamat, S. S. & Cravatt, B. F. A calcium-dependent acyltransferase that produces N-acyl phosphatidylethanolamines. *Nat. Chem. Biol.* 1–5 (2016). doi:10.1038/nchembio.2127

20. Cadas, H., di Tomaso, E. & Piomelli, D. Occurrence and biosynthesis of endogenous cannabinoid precursor, N-arachidonoyl phosphatidylethanolamine, in rat brain. *J. Neurosci.* **17,** 1226–42 (1997).

21. Tsuboi, K. *et al.* Enzymatic formation of N-acylethanolamines from N-acylethanolamine plasmalogen through N-acylphosphatidylethanolamine-hydrolyzing phospholipase D-dependent and -independent pathways. *Biochim. Biophys. Acta - Mol. Cell Biol. Lipids* **1811,** 565–577 (2011).

22. Uyama, T. *et al.* Generation of N-acylphosphatidylethanolamine by members of the phospholipase A/acyltransferase (PLA/AT) family. *J. Biol. Chem.* **287,** 31905–31919 (2012).

23. Ueda, N., Tsuboi, K. & Uyama, T. Enzymological studies on the biosynthesis of N-acylethanolamines. *Biochimica et Biophysica Acta - Molecular and Cell Biology of Lipids* **1801,** 1274–1285 (2010).

24. Okamoto, Y., Morishita, J., Tsuboi, K., Tonai, T. & Ueda, N. Molecular Characterization of a Phospholipase D Generating Anandamide and Its Congeners. *J. Biol. Chem.* **279,** 5298–5305 (2004).

25. Magotti, P. *et al.* Structure of human NAPE-PLD: regulation of fatty-acid ethanolamide biosynthesis by bile acids. *Structure* **23,** 598–604 (2015).

26. Zhu, C. *et al.* Proinflammatory stimuli control NAPE-PLD expression in macrophages. *Mol Pharmacol* (2011). doi:mol.110.070201 [pii]\r10.1124/mol.110.070201 [doi]

27. Natarajan, V., Schmid, P. C., Reddy, P. V. & Schmid, H. H. O. Catabolism of N-Acylethanolamine Phospholipids by Dog Brain Preparations. *J. Neurochem.* **42,** 1613–1619 (1984).

28. Leung, D., Saghatelian, A., Simon, G. M. & Cravatt, B. F. Inactivation of N-acyl phosphatidylethanolamine phospholipase D reveals multiple mechanisms for the biosynthesis of endocannabinoids. *Biochemistry* **45,** 4720–4726 (2006).

29. Simon, G. M. & Cravatt, B. F. Endocannabinoid biosynthesis proceeding through glycerophospho-N-acyl ethanolamine and a role for alpha/beta hydrolase 4 in this pathway. *J. Biol. Chem.* **281,** 26465–26472 (2006).

30. Simon, G. M. & Cravatt, B. F. Characterization of mice lacking candidate N-acyl ethanolamine biosynthetic enzymes provides evidence for multiple pathways that contribute to endocannabinoid production in vivo. *Mol. Biosyst.* **6,** 1411–8 (2010).

31. Liu, J. *et al.* A biosynthetic pathway for anandamide. *Proc. Natl. Acad. Sci. U. S. A.* **103,** 13345–50 (2006).

32. Shiratsuchi, A. *et al.* Inhibitory effect of N-palmitoylphosphatidylethanolamine on macrophage phagocytosis through inhibition of Rac1 and Cdc42. *J. Biochem.* **145,** 43–50 (2009).

33. Epps, D. E., Natarajan, V., Schmid, P. C. & Schmid, H. H. O. Accumulation of N-acylethanolamine glycerophospholipids in infarcted myocardium. *Biochim. Biophys. Acta (BBA)/Lipids Lipid Metab.* **618,** 420–430 (1980).

34. Kondo, S. *et al.* Accumulation of various n-acylethanolamines including N-arachidonoylethanolamine (anandamide) in cadmium chloride-administered rat testis. *Arch. Biochem. Biophys.* **354,** 303–310 (1998).

35. Schmid, P. C., Paria, B. C., Krebsbach, R. J., Schmid, H. H. & Dey, S. K. Changes in anandamide levels in mouse uterus are associated with uterine receptivity for embryo implantation. *Proc. Natl. Acad. Sci. U. S. A.* **94,** 4188–92 (1997).

36. Moesgaard, B., Petersen, G., Jaroszewski, J. W. & Hansen, H. S. Age dependent accumulation of N-acyl-ethanolamine phospholipids in ischemic rat brain. A (31)P NMR and enzyme activity study. *J. Lipid Res.* **41,** 985–90 (2000).

37. Hansen, H. S. *et al.* Characterization of glutamate-induced formation of N-acylphosphatidylethanolamine and N-acylethanolamine in cultured neocortical neurons. *J. Neurochem.* **69,** 753–61 (1997).

38. Berger, C. *et al.* Massive accumulation of N-acylethanolamines after stroke. Cell signalling in acute cerebral ischemia? *J. Neurochem.* **88,** 1159–1167 (2004).

39. Janfelt, C. *et al.* Visualization by mass spectrometry of 2-dimensional changes in rat brain lipids, including N-acylphosphatidylethanolamines, during neonatal brain ischemia. *FASEB J.* **26,** 2667–2673 (2012).

40. Di Marzo, V. *et al.* Formation and inactivation of endogenous cannabinoid anandamide in central neurons. *Nature* **372,** 686–691 (1994).

41. Cadas, H., Gaillet, S., Beltramo, M., Venance, L. & Piomelli, D. Biosynthesis of an endogenous cannabinoid precursor in neurons and its control by calcium and cAMP. *J.Neurosci.* **16,** 3934–3942 (1996).

42. Parkinson, J. An essay on the shaking palsy. 1817. *J. Neuropsychiatry Clin. Neurosci.* **14,** 223–36; discussion 222 (2002).

43. Carlsson, A., Lindqvist, M., Magnusson, T. & Waldeck, B. On the presence of 3-hydroxytyramine in brain. *Science (80-.).* **127,** 471 (1958).

44. Goetz, C. G. The history of Parkinson's disease: Early clinical descriptions and neurological therapies. *Cold Spring Harb. Perspect. Med.* **1,** (2011).

45. Nutt, J. & Wooten, G. F. Clinical Practice. Diagnosis and initial management of Parkinson's disease. *N. Engl. J. Med.* **353,** 1021–1027 (2005).

46. Ascherio, A. & Schwarzschild, M. A. The epidemiology of Parkinson's disease: risk factors and prevention. *The Lancet Neurology* **15,** 1257–1272

(2016).

47. Dauer, W. & Przedborski, S. Parkinson's disease: mechanisms and models. *Neuron* **39,** 889–909 (2003).

48. Martin, Dawson, V. L. & Dawson, T. M. The impact of genetic research on our understanding of Parkinson's disease. *Prog. Brain Res.* **183,** 21–41 (2010).

49. Greenamyre, J. T. & Hastings, T. G. Biomedicine. Parkinson's--divergent causes, convergent mechanisms. *Science* **304,** 1120–1122 (2004).

50. Hirsch, E. C. & Hunot, S. Neuroinflammation in Parkinson's disease: a target for neuroprotection? *The Lancet Neurology* **8,** 382–397 (2009).

51. Olanow, C. W., Stern, M. B. & Sethi, K. The scientific and clinical basis for the treatment of Parkinson disease (2009). *Neurology* **72,** (2009).

52. Jenner, P. & Olanow, C. W. Oxidative stress and the pathogenesis of Parkinson's disease. *Neurology* **47,** S161–S170 (1996).

53. Liang, C. L., Wang, T. T., Luby-Phelps, K. & German, D. C. Mitochondria mass is low in mouse substantia nigra dopamine neurons: Implications for Parkinson's disease. *Exp. Neurol.* **203,** 370–380 (2007).

54. Van Laar, V. S. & Berman, S. B. Mitochondrial dynamics in Parkinson's disease. *Experimental Neurology* **218,** 247–256 (2009).

55. Yu, W., Sun, Y., Guo, S. & Lu, B. The PINK1/Parkin pathway regulates mitochondrial dynamics and function in mammalian hippocampal and dopaminergic neurons. *Hum. Mol. Genet.* **20,** 3227–3240 (2011).

56. Bendor, J. T., Logan, T. P. & Edwards, R. H. The function of alpha-synuclein. *Neuron* **79,** 1044–1066 (2013).

57. Lindersson, E. *et al.* Proteasomal Inhibition by α-Synuclein Filaments and Oligomers. *J. Biol. Chem.* **279,** 12924–12934 (2004).

58. Höglinger, G. U. *et al.* Dysfunction of mitochondrial complex I and the proteasome: interactions between two biochemical deficits in a cellular model of Parkinson's disease. *J. Neurochem.* **86,** 1297–1307 (2003).

59. Manning-Bog, A. B. *et al.* The herbicide paraquat causes up-regulation and aggregation of alpha-synuclein in mice: Paraquat and alpha-synuclein. *J. Biol. Chem.* **277,** 1641–1644 (2002).

60. Mercado, G., Valdés, P. & Hetz, C. An ERcentric view of Parkinson's disease. *Trends in Molecular Medicine* **19,** 165–175 (2013).

61. Jiang, P. *et al.* ER stress response plays an important role in aggregation of α-synuclein. *Mol. Neurodegener.* **5,** 56 (2010).

62. Mosley, R. L., Hutter-Saunders, J. A., Stone, D. K. & Gendelman, H. E. Inflammation and adaptive immunity in Parkinson's disease. *Cold Spring Harb. Perspect. Med.* **2,** (2012).

63. Ransohoff, R. M. How neuroinflammation contributes to neurodegeneration. *Science (80-.).* **353,** 777–83 (2016).

64. Good, C. H. *et al.* Impaired nigrostriatal function precedes behavioral deficits in a genetic mitochondrial model of Parkinson's disease. *FASEB J. Off. Publ. Fed. Am. Soc. Exp. Biol.* **25,** 1333–1344 (2011).

65. Gubellini, P. & Kachidian, P. Animal models of Parkinson's disease: An updated overview. *Revue Neurologique* **171,** 750–761 (2015).

66. Mayer, R. A., Kindt, M. V. & Heikkila, R. E. Prevention of the Nigrostriatal Toxicity of 1-Methyl-4-Phenyl-1,2,3,6-Tetrahydropyridine by Inhibitors of 3,4-Dihydroxyphenylethylamine Transport. *J. Neurochem.* **47,** 1073–1079 (1986).

67. Nicklas, W. m dotJ, Vyas, I. & Heikkila, R. E. Inhibition of NADH-linked oxidation in brain mitochondria by 1-methyl-4-phenyl-pyridine, a metabolite of the neurotoxin, 1-methyl-4-phenyl-1,2,5,6-tetrahydropyridine. *Life Sci.* **36,** 2503–2508 (1985).

68. Gubellini, P., Picconi, B., Di Filippo, M. & Calabresi, P. Downstream mechanisms triggered by mitochondrial dysfunction in the basal ganglia: From experimental models to neurodegenerative diseases. *Biochimica et Biophysica Acta - Molecular Basis of Disease* **1802,** 151–161 (2010).

69. Betarbet, R. *et al.* Chronic systemic pesticide exposure reproduces features of Parkinson's disease. *Nat. Neurosci.* **3,** 1301–1306 (2000).

70. Shimizu, K. *et al.* Carrier-mediated processes in blood-brain barrier penetration and neural uptake of paraquat. *Brain Res.* **906,** 135–142 (2001).

71. Cochemé, H. M. & Murphy, M. P. Complex I is the major site of mitochondrial superoxide production by paraquat. *J. Biol. Chem.* **283,** 1786–1798 (2008).

72. Takahashi, R. N., Rogerio, R. & Zanin, M. Maneb enhances MPTP neurotoxicity in mice. *Res. Commun. Chem. Pathol. Pharmacol.* **66,** 167–170 (1989).

73. Ungerstedt, U. 6-Hydroxy-dopamine induced degeneration of central monoamine neurons. *Eur. J. Pharmacol.* **5,** 107–110 (1968).

74. Soto-Otero, R., Méndez-Álvarez, E., Hermida-Ameijeiras, Á., Muñoz-Patiño, A. M. & Labandeira-Garcia, J. L. Autoxidation and neurotoxicity of 6-hydroxydopamine in the presence of some antioxidants: Potential implication in relation to the pathogenesis of Parkinson's disease. *J. Neurochem.* **74,** 1605–1612 (2000).

75. Borisenko, G. G., Kagan, V. E., Hsia, C. J. C. & Schor, N. F. Interaction between 6-hydroxydopamine and transferrin: 'Let my iron go'. *Biochemistry* **39,** 3392–3400 (2000).

76. Glinka, Y. Y. & Youdim, M. B. H. Inhibition of mitochondrial complexes I and IV by 6-hydroxydopamine. *Eur. J. Pharmacol. Environ. Toxicol.* **292,** 329–332 (1995).

77. Woodgate, A., MacGibbon, G., Walton, M. & Dragunow, M. The toxicity of 6-hydroxydopamine on PC12 and P19 cells. *Mol. Brain Res.* **69,** 84–92 (1999).

78. Jeon, B. S., Jackson-Lewis, V. & Burke, R. E. 6-Hydroxydopamine lesion of the rat substantia nigra: time course and morphology of cell death. *Neurodegeneration* **4,** 131–137 (1995).

79. Sarre, S. *et al.* In vivo characterization of somatodendritic dopamine release in the substantia nigra of 6-hydroxydopamine-lesioned rats. *J. Neurochem.* **90,** 29–39 (2004).

80. Przedbroski, S. *et al.* Dose-dependent lesions of the dopaminergic nigrostriatal pathway induced by instrastriatal injection of 6-hydroxydopamine. *Neuroscience* **67,** 631–647 (1995).

81. Marinova-Mutafchieva, L. *et al.* Relationship between microglial activation and dopaminergic neuronal loss in the substantia nigra: A time course study in a 6-hydroxydopamine model of Parkinson's disease. *J. Neurochem.* **110,** 966–975 (2009).

82. Ungerstedt, U. & Arbuthnott, G. W. Quantitative recording of rotational behavior in rats after 6-hydroxy-dopamine lesions of the nigrostriatal dopamine system. *Brain Res.* **24,** 485–493 (1970).

83. Tieu, K. A guide to neurotoxic animal models of Parkinson's disease. *Cold Spring Harb. Perspect. Med.* **1,** (2011).

84. Joel, D. & Weiner, I. The connections of the dopaminergic system with the striatum in rats and primates: An analysis with respect to the functional and compartmental organization of the striatum. *Neuroscience* **96,** 451–474 (2000).

85. Brooks, S. P. & Dunnett, S. B. Tests to assess motor phenotype in mice: a user's guide. *Nat. Rev. Neurosci.* **10,** 519–29 (2009).

86. Iancu, R., Mohapel, P., Brundin, P. & Paul, G. Behavioral characterization of a unilateral 6-OHDA-lesion model of Parkinson's disease in mice. *Behav. Brain Res.* **162,** 1–10 (2005).

87. Brooks, S. P. & Dunnett, S. B. Tests to assess motor phenotype in mice: a user's guide. *Nat. Rev. Neurosci.* **10,** 519–29 (2009).

88. Stoppini, L., Buchs, P.-A. & Muller, D. A simple method for organotypic cultures of nervous tissue. *J. Neurosci. Methods* **37,** 173–182 (1991).

89. Falkenburger, B. H. & Schulz, J. B. Limitations of cellular models in Parkinson's disease research. *J. Neural Transm. Suppl.* 261–8 (2006). doi:Review

90. Soldner, F. *et al.* Parkinson's Disease Patient-Derived Induced Pluripotent Stem Cells Free of Viral Reprogramming Factors. *Cell* **136,** 964–977 (2009).

91. Xie, H., Hu, L. & Li, G. SH-SY5Y human neuroblastoma cell line: in vitro cell model of dopaminergic neurons in Parkinson's disease. *Chin. Med. J. (Engl).* **123,** 1086–1092 (2010).

92. Pandey, N., Schmidt, R. E. & Galvin, J. E. The alpha-synuclein mutation E46K promotes aggregation in cultured cells. *Exp. Neurol.* **197,** 515–520 (2006).

93. Xin, W. *et al.* Toxic Oligomeric Alpha-Synuclein Variants Present in Human Parkinson's Disease Brains Are Differentially Generated in Mammalian Cell Models. *Biomolecules* **5,** 1634–1651 (2015).

94. Constantinescu, R., Constantinescu, A. T., Reichmann, H. & Janetzky, B. Neuronal differentiation and long-term culture of the human neuroblastoma line SH-SY5Y. *J Neural Transm* 17–28 (2007).

95. Cernaianu, G. *et al.* All-trans retinoic acid arrests neuroblastoma cells in a dormant state. Subsequent nerve growth factor/brain-derived neurotrophic factor treatment adds modest benefit. *J. Pediatr. Surg.* **43,** 1284–1294 (2008).

96. Pfaffl, M. W., Tichopad, A., Prgomet, C. & Neuvians, T. P. Determination of stable housekeeping genes, differentially regulated target genes and sample integrity: BestKeeper--Excel-based tool using pair-wise correlations. *Biotechnol Lett* **26,** 509–515 (2004).

97. Falkenburger, B. H. & Schulz, J. B. Limitations of cellular models in Parkinson's disease research. *J. Neural Transm. Suppl.* 261–8 (2006). doi:Review

98. Esteves, A. R. & Cardoso, S. M. LRRK2 at the Crossroad Between Autophagy and Microtubule Trafficking: Insights into Parkinsons Disease.

Neurosci. (2016). doi:10.1177/1073858415616558

99. Chan, D., Citro, A., Cordy, J. M., Shen, G. C. & Wolozin, B. Rac1 protein rescues neurite retraction caused by G2019s leucine-rich repeat kinase 2 (LRRK2). *J. Biol. Chem.* **286,** 16140–16149 (2011).

100. Stankiewicz, T. R. & Linseman, D. a. Rho family GTPases: key players in neuronal development, neuronal survival, and neurodegeneration. *Front. Cell. Neurosci.* **8,** 314 (2014).

101. Stępkowski, T. M., Wasyk, I., Grzelak, A. & Kruszewski, M. 6-OHDA-Induced Changes in Parkinson`s Disease-Related Gene Expression are not Affected by the Overexpression of PGAM5 in In Vitro Differentiated Embryonic Mesencephalic Cells. *Cell. Mol. Neurobiol.* **35,** 1137–1147 (2015).

102. Duke, D. C. *et al.* Transcriptome analysis reveals link between proteasomal and mitochondrial pathways in Parkinson's disease. *Neurogenetics* **7,** 139–148 (2006).

103. Magalingam, K. B., Radhakrishnan, A., Ramdas, P. & Haleagrahara, N. Quercetin glycosides induced neuroprotection by changes in the gene expression in a cellular model of Parkinson's disease. *J. Mol. Neurosci.* **55,** 609–17 (2015).

104. Rekha, K. R. & Selvakumar, G. P. Gene expression regulation of Bcl2, Bax and cytochrome-C by geraniol on chronic MPTP/probenecid induced C57BL/6 mice model of Parkinson's disease. *Chem. Biol. Interact.* **217,** 57–66 (2014).

105. Abdelkader, N. F., Safar, M. M. & Salem, H. A. Ursodeoxycholic Acid Ameliorates Apoptotic Cascade in the Rotenone Model of Parkinson's Disease: Modulation of Mitochondrial Perturbations. *Mol. Neurobiol.* **53,** 810–817 (2016).

106. Moran, J. M. *et al.* Identification of genes associated with paraquat-induced toxicity in SH-SY5Y cells by PCR array focused on apoptotic pathways. *J. Toxicol. Environ. Health. A* **71,** 1457–1467 (2008).

107. Grünblatt, E. *et al.* Gene expression profiling of parkinsonian substantia nigra pars compacta; alterations in ubiquitin-proteasome, heat shock protein, iron and oxidative stress regulated proteins, cell adhesion/cellular matrix and vesicle trafficking genes. *J. Neural Transm.* **111,** 1543–1573 (2004).

108. Ohnuki, T., Nakamura, A., Okuyama, S. & Nakamura, S. Gene expression profiling in progressively MPTP-lesioned macaques reveals molecular pathways associated with sporadic Parkinson's disease. *Brain Res.* **1346,** 26–42 (2010).

109. Jin, S. M. & Youle, R. J. The accumulation of misfolded proteins in the mitochondrial matrix is sensed by PINK1 to induce PARK2/Parkin-mediated mitophagy of polarized mitochondria. *Autophagy* **9,** 1750–1757 (2013).

110. Sandebring, A. *et al.* Parkin deficiency disrupts calcium homeostasis by modulating phospholipase C signalling. *FEBS J.* **276,** 5041–5052 (2009).

111. Vercammen, L. *et al.* Parkin Protects against Neurotoxicity in the 6-Hydroxydopamine Rat Model for Parkinson's Disease. *Mol. Ther.* **14,** 716–723 (2006).

112. Dagda, R. K. *et al.* Loss of PINK1 function promotes mitophagy through effects on oxidative stress and mitochondrial fission. *J. Biol. Chem.* **284,** 13843–13855 (2009).

113. Simunovic, F. *et al.* Gene expression profiling of substantia nigra dopamine neurons: further insights into Parkinson's disease pathology. *Brain* **132,** 1795–1809 (2009).

114. Schreij, A. M. *et al.* LRRK2 localizes to endosomes and interacts with clathrin-light chains to limit Rac1 activation. *EMBO Rep.* **16,** 79–86 (2015).

115. Esteves, A. R., Swerdlow, R. H. & Cardoso, S. M. LRRK2, a puzzling protein: Insights into Parkinson's disease pathogenesis. *Experimental Neurology* **261,** 206–216 (2014).

116. Hordijk, P. L. Regulation of NADPH oxidases: The role of Rac proteins. *Circulation Research* **98,** 453–462 (2006).

117. Nikolova, S., Lee, Y. S., Lee, Y.-S. & Kim, J. Rac1-NADPH oxidase-regulated generation of reactive oxygen species mediates glutamate-induced apoptosis in SH-SY5Y human neuroblastoma cells. *Free Radic. Res.* **39,** 1295–304 (2005).

118. Barth, B. M., Stewart-Smeets, S. & Kuhn, T. B. Proinflammatory cytokines provoke oxidative damage to actin in neuronal cells mediated by Rac1 and NADPH oxidase. *Mol. Cell. Neurosci.* **41,** 274–285 (2009).

119. Kim, G. S., Jung, J. E., Niizuma, K. & Chan, P. H. CK2 is a novel negative regulator of NADPH oxidase and a neuroprotectant in mice after cerebral ischemia. *J. Neurosci.* **29,** 14779–89 (2009).

120. Meng, S., Su, Z., Liu, Z., Wang, N. & Wang, Z. Rac1 contributes to cerebral ischemia reperfusion-induced injury in mice by regulation of Notch2. *Neuroscience* **306,** 100–114 (2015).

121. Chang, F., Lemmon, C.A., Park, D., et al. FAK Potentiates Rac1 Activation and Localization to Matrix Adhesion Sites: A Role for BPix. *Mol. Biol. Cell* **18,** 253–264 (2007).